JOURNAL OF GEOPHYSICAL RESEARCH, VOL. 104, NO. D4, PAGES 4005–4024, FEBRUARY 27, 1999

Atmospheric sulfur and deep convective clouds in tropical Pacific: A model study

C. Andronache, [1] L. J. Donner, C. J. Seman, V. Ramaswamy,
and R. S. Hemler
Geophysical Fluid Dynamics Laboratory, NOAA, Princeton University, Princeton, New Jersey

Abstract. A high-resolution limited area nonhydrostatic model was used to simulate sulfate-cloud interactions during the convective activity in a case study from the Tropical Ocean Global Atmosphere Coupled Ocean Atmosphere Response Experiment, December 20-25, 1992. The model includes a new detailed sulfate-cloud microphysics scheme designed to estimate the effects of sulfate on cloud microphysics and radiative properties and the effects of deep convection on the transport and redistribution of aerosol. The data for SO_2 and $SO_4^{(2-)}$ species were taken from the Pacific Exploratory Mission West B observations during February-March 1994. Results show that a change in sulfate loading from the minimum to the maximum observed value scenarios (i.e., from about 0.01 to 1 μg m^{-3}) causes a significant decrease of the effective radius of cloud droplets (changes up to 2 μm on average) and an increase of the diagnostic number concentration of cloud droplets (typical changes about 5-20 cm^{-3}). The change in the average net shortwave (SW) radiation flux above the clouds was estimated to be on average -1.5 W m^{-2}, with significant spatial and temporal variations. The horizontal average of the changes in the net SW radiation fluxes above clouds has a diurnal cycle, reaching typical values approximately -3 W m^{-2}. The changes in the average net longwave radiation flux above the clouds were negligible, but they showed significant variations, typically between -10 W m^{-2} and 10 W m^{-2} near the surface. These variations were associated mainly with the changes in the distribution of cloud water, which showed typical relative changes of cloud water path of about 10-20%. Other notable changes induced by the increase of aerosol were the variations in air temperature of the order of 1°C. The case study presented here suggests that characteristics of convective clouds in tropical areas are sensitive to atmospheric sulfate loading, particularly during enhanced sulfate episodes.

1. Introduction

Sulfate aerosol is produced by oxidation of sulfur compounds and is regarded as a significant factor in the climate system, particularly because major anthropogenic perturbations [*Penner et al.*, 1994; *Intergovernmental Panel on Climate Change (IPCC)*, 1995]. It has been shown that the atmospheric sulfate aerosols interact with solar radiation and can change the microphysical properties of clouds. The scatter of solar radiation back to space or the direct radiative forcing (DRF) by sulfate aerosols is estimated between -0.3 and -0.9 W m^{-2} as a global average [*Charlson et al.*, 1992; *Kiehl and Briegleb*, 1993]. Further refinements of DRF estimates include the effects of carbonaceous particles, which absorb solar radiation and tend to reduce the cooling effect of sulfate aerosol. However, recent evaluations of the combined effects of sulfate and carbonaceous particles suggest a significant average net negative forcing upon the global atmosphere [*Haywood and Shine*, 1995].

In addition to the DRF, sulfate aerosols interact with clouds, primarily by providing cloud condensation nuclei (CCN). An increase of atmospheric sulfate concentration produces an increase in CCN concentration, a fact well documented by in situ observations [*Leaitch et al.*, 1992; *Leaitch and Isaac*, 1994; *Quinn et al.*, 1993; *Hegg et al.*, 1993; *Hegg*, 1994; *King et al.*, 1993; *Van Dingenen et al.*, 1995]. Because the microphysical processes involved in the activation of "dry" aerosol to CCN are not fully understood, the current modeling studies of aerosol-cloud interactions employ an empirical relationship between sulfate concentration and

[1]Atmospheric and Oceanic Sciences Program, Princeton University, Princeton, New Jersey

Paper number 1998JD200085.
0148-0227/99/1998JD200085$09.00

CCN concentration [*Boucher and Rodhe*, 1994; *Boucher and Lohmann*, 1995; *IPCC*, 1995; *Jones and Slingo*, 1996]. CCN concentration, in turn, determines the cloud droplet concentration and influences the size of droplets. For the same humidity and updraft velocity conditions, more CCN lead to higher concentrations of droplets with a smaller average size [*Twomey*, 1974, 1977; 1990; *Hobbs*, 1993]. As a result, the distribution of radiative fluxes in the cloudy area and the cloud albedo might change owing to the presence of sulfate aerosol causing an indirect radiative forcing (IRF) [*Slingo*, 1989; *Boucher and Lohmann*, 1995; *Jones and Slingo*, 1996; *Chaung et al.*, 1997]. The IRF was estimated by *Jones and Slingo* [1996] between -0.5 and -1.5 W m^{-2} as a global average, while *Boucher and Rodhe* [1994] estimated the same effect between -0.7 and -1.4 W m^{-2}. Using a global model with coupled sulfur and cloud microphysics, *Lohmann and Feichter* [1997] found a global average of IRF of -2.2 Wm^{-2}, with significant regional variability. While there are still uncertainties in the current IRF evaluation, all these studies suggest that on average the indirect effect of sulfate aerosol is to enhance the global cloud albedo.

Most of the previous studies of IRF focused on stratocumulus clouds because of their potentially important role in the climate system on a global basis. The deep convective clouds were neglected or treated in a simplified manner in these climate models. For tropical areas (between 30°S and 30°N), *Warren et al.* [1986; 1988] show that the annual-zonal average cloud amounts are ~6% for cumulonimbus clouds, 21% for stratus, stratocumulus clouds, and fog combined, and 14% for cirrus, cirrostratus and cirrocumulus clouds combined. A significant fraction of cirrus clouds in tropical area is likely to be connected to convective transport of water into upper troposphere, and this fraction is comparable with the average coverage of stratiform clouds. In addition, the solar energy per unit time at the top of the atmosphere intercepted by the tropical area (between 30°S and 30°N) represents ~60% of the total solar energy intercepted by Earth. Therefore the importance of the indirect radiative effects of cumulonimbus and cirrus cloud systems in tropical areas can be significant and requires further investigation.

In addition, recent studies indicate that deep convective clouds play a major role in transporting tracers from the boundary layer (BL) into the upper troposphere [*Chatfield and Crutzen*, 1984; *Flossmann*, 1991; *Wang et al.*, 1995; *Taylor et al.*, 1997]. The effect of convective motions on gaseous and particulate species are transport of species from the BL to higher altitudes by convective motions (cloud pumping); precipitation scavenging; heterogeneous chemical reactions occurring in cloud droplets, sometimes much faster than the reactions in gas phase [*Chameides and Davis*, 1982; *Giorgi and Chameides*, 1986; *Langner and Rodhe*, 1991; *Hegg et al.*, 1984, 1996; *Chin et al.*, 1996; *Taylor et al.*, 1997]. It is conceivable that the transport of sulfur species and sulfur conversion in clouds might affect the cloud microphysics and the radiative properties of these types of clouds, which have spatially extensive anvils in which indirect radiative effects could manifest.

In this study, we use the high-resolution Geophysical Fluid Dynamics Laboratory (GFDL) limited area nonhydrostatic (LAN) model to address the problem of the effect of sulfate upon the cloud microphysics and the radiative fluxes in tropical convective systems. In contrast with most of the previous studies that addressed this problem with general circulation models in which average conditions and coarse resolution were used, we formulate simulations with detailed dynamics of convection driven by observations during Tropical Ocean Global Atmosphere Coupled Ocean Atmosphere Response Experiment (TOGA COARE) and with sulfate chemistry driven by observations during Pacific Exploratory Mission in the western Pacific Ocean, phase B (PEM-West B) [*Andronache et al.*, 1998]. The results reported in this work provide new insights into the mechanism of sulfate-cloud interactions in tropical convective systems with implications for the impact of sulfate loading on the microphysical and radiative properties of clouds.

2. Method

The LAN model developed at GFDL is a three-dimensional high-resolution dynamic model designed for studies of convective clouds and radiative-convective equilibrium [*Lipps and Hemler*, 1986; *Held et al.*, 1993; *Haywood et al.*, 1997; *Andronache et al.*, 1998; *Donner et al.*, 1998]. The model provides a framework for studies of deep convection and employs physics typical for a high resolution mesoscale model (for details, see *Held et al.* [1993]). The cloud physics scheme in LAN predicts the water concentration in gas phase, cloud droplets, snow, and rain. The radiation code is a 56-band two-stream δ-Eddington scheme, modified to include gaseous absorption and a parameterization for Rayleigh scattering and cloud optical properties [*Ramaswamy and Kiehl*, 1985; *Slingo*, 1989]. A two-dimensional version of the GFDL LAN model is used in this study. This version has a spatial resolution of 2 km in the horizontal and 500 m in the vertical. The horizontal extension of the domain is 512 km, and the vertical extension is up to 21 km. The cloud microphysics and sulfate schemes, the relationship between CCN and sulfate, and the initial and boundary conditions are discussed below.

2.1. Cloud Microphysics and Radiation

The model employs bulk cloud physics, with prognostic equations for the mixing ratios of four variables of interest: water vapor concentration, q_v, cloud water/ice concentration, q_c, rainwater, q_r, and ice/snow concentration, q_s. Figure 1 shows the scheme of cloud microphysics processes included in LAN. For tempera-

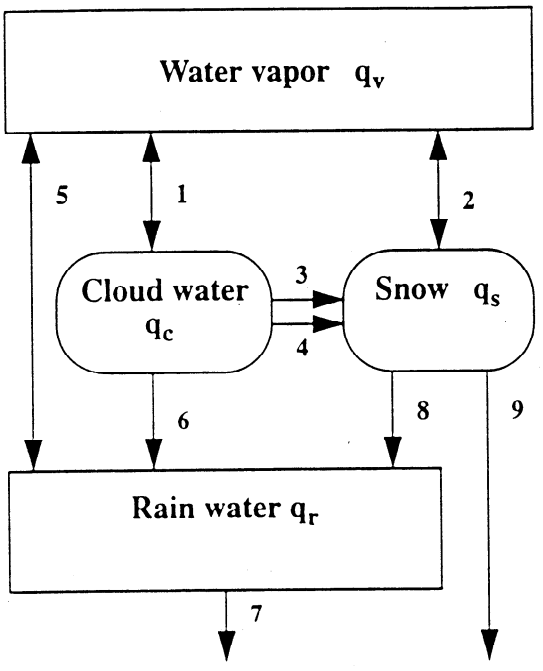

Figure 1. Cloud physics scheme included in the GFDL LAN model. The processes indicated by arrows correspond to condensation (evaporation) of cloud droplets (1), deposition (sublimation) of vapor to snow (2), autoconversion of cloud droplets into snow (3), accretion of cloud droplets into snow (4), evaporation (condensation) of vapors into rain droplets (5), accretion of cloud droplets into rain drops (6), rainfall (7), snowmelt (8), and snowfall (9).

tures higher than -6°C, q_c is assumed to be only cloud water, and the latent heat of vaporization is released at condensation. For temperatures less than -12°C, q_c is assumed to be only ice, and the latent heat of sublimation is released at condensation. At intermediate temperatures, a mixture of cloud water and ice are assumed, with the percentage of each varying linearly with temperature [*Lord et al.*, 1984]. The prognostic equations for each variable and the assumptions made in the parameterization of the main physical processes are described in detail by *Held et al.* [1993]. The model was used in previous studies to simulate the convective activity and the water cycle for the Global Atmosphere Tropical Experiment (GATE) and TOGA COARE data and provided good agreement with observations [*Lipps and Hemler*, 1986; *Haywood et al.*, 1997; *Donner et al.*, 1998].

An important parameter needed for the description of the radiative properties of clouds is the cloud droplet effective radius, r_e. This parameter is used along with the cloud water path (CWP) to define the single-scattering properties of clouds. For each spectral interval, i, the optical thickness, τ_i, the single-scattering albedo, $\tilde{w}_i$, and the asymmetry parameter, g_i, can be linked to CWP and r_e [*Slingo*, 1989]. The effective radius is given by

$$r_e = \frac{\int_0^\infty r^3 n(r)dr}{\int_0^\infty r^2 n(r)dr} \quad (1)$$

or $r_e=(\bar{r^3})/(\bar{r^2})$, where r is the cloud droplet radius and $n(r)$ is the droplet size distribution. In this work, we assume a Khrigian-Mazin size distribution for cloud droplets and a Marshall-Palmer distribution for the rain drops [see *Pruppacher*, 1981].

The parameterization of cloud radiative properties developed by *Slingo* [1989] was used successfully in general circulation models (GCMs) and other models treating the effects of cloud microphysics on radiation [*Held et al.*, 1993; *Kiehl and Briegleb*, 1993; *Jones and Slingo*, 1996]. This parameterization is based on a simple relationship between r_e and the average cloud droplet radius, $\bar{r}=\int_0^\infty rn(r)dr/\int_0^\infty n(r)dr$, deduced from observations and theoretical considerations as summarized in this section. In turn, $\bar{r}$ can be expressed in terms of water content and concentration of cloud droplets.

To analyze the existence and validity of a relationship between r_e and the droplet average radius, $\bar{r}$, we start from the general expression $r_e=f(\bar{r})$, which is not restrictive a priori. This relation can be obtained by expressing $r_e=(\bar{r^3})/(\bar{r^2})$ in terms of $\bar{r}$ and a standard deviation of r. It can be shown that $\bar{r^2}=(\bar{r})^2(1+d^2)$, where $d=\sigma/\bar{r}$ is the spectral dispersion of the drop-size distribution (σ is the standard deviation and $\bar{r}$ is the average radius). The liquid water content $q_c\rho_a$ is related to the size distribution by $q_c\rho_a=\int_0^\infty \rho_w(4\pi r^3/3)n(r)dr$, where ρ_a is the density of air and ρ_w is the density of water. If N_d is the total number concentration of cloud droplets, then

$$\bar{r^3} = \frac{3q_c\rho_a}{4\pi\rho_w N_d} \quad (2)$$

and r_e becomes

$$r_e = K(d)\left(\frac{3q_c\rho_a}{4\pi\rho_w N_d}\right)^{1/3} \quad (3)$$

where $K(d)$ depends on the spectral dispersion and is given by $K(d)=(1+3d^2)^{2/3}/(1+d^2)$. Thus relation (3) can be written as $r_e=K(d)\bar{r}$, which is a general relationship because nothing was assumed about the form of the drop-size distribution. The next step is to evaluate K and its variability based on observations and theoretical considerations for different types of clouds and conditions.

For a Khrigian-Mazin cloud droplet size distribution [see *Pruppacher*, 1981], it can be shown that K=1.19. *Pontikis and Hicks* [1992] found $K\sim$(1-1.1), with the most frequent values near $\sim$1.05, based on data from warm trade-wind cumuli. *Martin et al.* [1994] found a robust linear relationship $r_e=K\bar{r}$, with K=1.143 for continental clouds and K=1.077 for marine clouds, based

on analysis of stratocumulus clouds. They also showed that drizzle does not affect these results, but the relation between r_e and $\bar{r}$ is not linear in conditions of entrainment or precipitation. This situation is expected because the relation $r_e=K(d)\bar{r}$ is generally nonlinear and $K(d)$ depends on $\bar{r}$ and on the variability of drop-size distribution.

Alterations of the linear relationship between r_e and $\bar{r}$ are expected in the presence of entrainment, precipitation, and ice particles. In the case of entrainment, one expects a mixture of size distributions, with different histories (from, for example, updraft air and from downdraft air). The effect of this "mixing of distributions" is to produce a function $K(d)$ which might vary from sample to sample. *Blyth and Latham* [1991] investigated ice-free, summertime cumulus clouds affected by entrainment, and concluded that $r_e=K\bar{r}$ with $K\approx1$, regardless of how much the clouds are diluted and rendered inhomogeneous by entrainment.

In the case of precipitation, the size distribution of rain drops is characterized by much larger particles (with $\bar{r}\sim1$ mm). The most widely used rain size distribution is that of *Marshall and Palmer* [1948], which has the form $n(D)=N_0\exp(-\lambda D)$ with two parameters N_0 and λ. The mean diameter of rain drops is $\bar{D}=1/\lambda$, and the standard deviation of the drop diameter is $\sigma=1/\lambda$. Thus the spectral dispersion becomes $d=2$ and $K(d)=1.105$ not very different from the values found by *Pontikis and Hicks* [1992] and by *Martin et al.* [1994] from their analysis. The experimental difficulty in determining K directly from measurements in rainy clouds is that K varies in time and space, due to the variability of the rain drop distribution. These variations are restricted mainly between 1 and 1.25 (K has a maximum for $d=1$), and, on average, $K\sim1.1$. This argument applies for entrainment also because of the intrinsic bounds of K variations, which might explain why *Blyth and Latham* [1991] found $K\sim1$ for all conditions. In the case of ice clouds, the relationship between r_e and $\bar{r}$ can still be represented by a $r_e=K(d)\bar{r}$ under the assumption that r is an equivalent sphere to the ice crystal, while we note a lack of experimental data, and the uncertainties in $K(d)$ can be higher than in the case of liquid droplets. There is a great need for improvement in ice cloud measurements and model parameterizations, in order to understand the absolute values of cloud radiative properties [*McFarquhar and Heymsfield*, 1997].

In this study, we are concerned with the differences in model results induced by changes in aerosol sulfate, and we are less concerned with the absolute values of cloud optical properties. In these conditions, the use of relationship $r_e=K\bar{r}$ is justified as long as the errors in r_e caused by the uncertainty in K are smaller than the changes in r_e induced by aerosol perturbations. Denoting by $(\delta r_e)_{aerosol}$ the changes in r_e due to aerosol change, and by $(\delta r_e)_{error}$, the changes in r_e due to uncertainties in $K(d)$, we have $(\delta r_e)_{aerosol}>(\delta r_e)_{error}$ in order to have significant results. Note that $r_e=K\bar{r}$ can be written as $\ln(r_e)=\ln(K)+\ln(\bar{r})$, and, by differentiating, we have $\delta r_e/r_e=\delta K/K+\delta\bar{r}/\bar{r}$, as a measure of the relative error of r_e. Since $K\sim1$, $\delta K\sim0.05$ (based on our estimates and on the literature referenced above), $\delta\bar{r}\sim1$ μm, $\bar{r}\sim10$ μm, and $r_e\sim10$ μm (based on *Han et al.* [1994]), we estimate that $\delta r_e/r_e\sim0.1$ or $(\delta r_e)_{error}\sim1$ μm. Our model simulations give $(\delta r_e)_{aerosol}$ up to 2 μm, and, on average, $(\delta r_e)_{aerosol}\sim1$ μm, as will be shown later in section 3.4., and therefore the estimated changes in r_e caused by the considered aerosol increase can be significant. As will be shown later in section 3.4., the changes in cloud water concentration induced by sulfate aerosol are mostly in liquid clouds because of the stronger dependence of cloud droplets on the aerosol loading below the cloud base. This dependence becomes less significant in altitude due to the decay with height and because of collision processes. Thus it seems that the impact of these aerosols on ice clouds is small for the changes considered here and further studies need to include other aerosols able to become ice nuclei under atmospheric conditions.

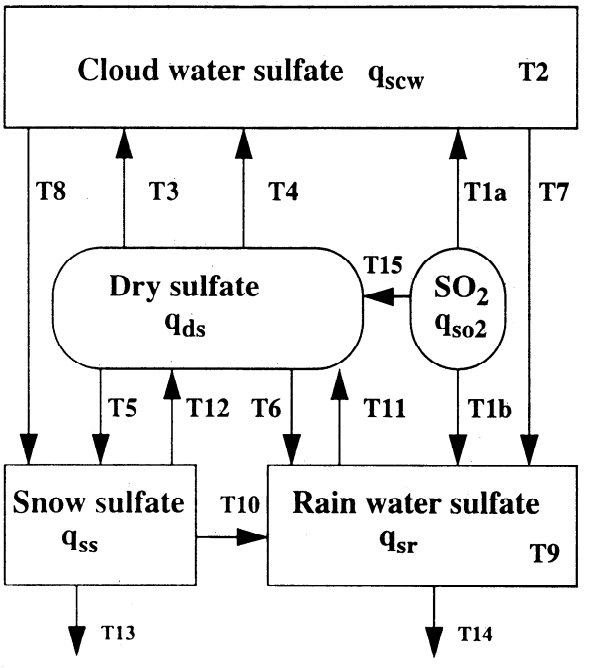

Figure 2. Sulfate-cloud interactions scheme included in the GFDL LAN model. The processes indicated by arrows correspond to absorption of gaseous SO_2 into the cloud and rain droplets (T1a, T1b), aqueous oxidation of SO_2 into the cloud and rain droplets (T2, T9), nucleation scavenging (T3), scavenging by Brownian diffusion (T4), dry scavenging (T5, T6), fluxes associated with autoconversion and accretion of cloud water droplets into rain drops and snow flakes (T7, T8), flux associated with the melt of snow (T10), flux associated with evaporation of rain drops (T11), flux associated with sublimation of snow (T12), fluxes associated to snowfall and rainfall (T13, T14), deposition of H_2SO_4 acid on dry sulfate (T15).

2.2. Sulfate-Cloud Interactions

The sulfate-cloud interaction model used in this work follows closely the concepts developed by *Hegg et al.* [1984] and is illustrated schematically in Figure 2. Five variables describing mixing ratios are treated explicitly in our model: the concentration of SO_2 in gas phase, q_{SO_2}; the concentration of "dry sulfate", or the sulfate in aerosol form, before activation and growth as a cloud droplet, q_{ds}; the sulfate concentration in liquid cloud droplets and ice crystals, q_{scw}; sulfate concentration in snow, q_{ss}; and the concentration of sulfate in rain droplets, q_{sr}. The absorption of SO_2, H_2O_2, and O_3 into the liquid cloud and rain droplets is described by the Henry's law, and the aqueous oxidation mechanism includes reactions of SO_2 with H_2O_2 and S(IV) with O_3 as a first approximation for the remote marine atmosphere [see *Penkett and Garland*, 1974; *Martin and Damschen*, 1981; *Hegg and Hobbs*, 1982; *Hegg et al.*, 1984; *Lin et al.*, 1992]. Initially, the oxidation of SO_2 by H_2O_2 takes place very efficiently in cloud droplets. However, H_2O_2 concentration is depleted due to its high solubility and due to oxidation with SO_2, and the aqueous oxidation of SO_2 by O_3 becomes an important pathway [*Seigneur and Saxena*, 1988]. Measurements of gaseous H_2O_2 in tropical Pacific [*Hoell et al.*, 1997; *Talbot et al.*, 1997] show that typical levels are in the range ~0.1-1.0 parts per billion by volume (ppbv), with an average value of 0.8 ppbv for the subset of data used here. Measured values of gaseous O_3 in the same region are in the range 10-100 ppbv with the most frequent values ~50 ppbv and an average value of 38 ppbv for the data used here (Figure 3). In the runs presented in this work, we maintain a constant O_3 concentration of 38 ppbv during integration and assume a decay timescale, $\tau(H_2O_2)$=4 hours, for H_2O_2 due to the decrease of H_2O_2 by absorption in cloud droplets and due to reaction with aqueous SO_2 [*Russell et al.*, 1994]. In the cloudless regions, H_2O_2 concentration is relaxed to the average value of 0.8 ppbv determined for the tropical western Pacific regions, based on the PEM-West B data.

The nucleation scavenging of dry aerosol by cloud droplets is the main process of depleting aerosol and its incorporation into cloud droplets by the process of activation. This process is effective for CCN under conditions of supersaturation. The process is dependent on aerosol size, chemical properties of the surface, solubility, and ambient relative humidity, and is generally difficult to include as an explicit mechanism in current models. However, experiments show that the fraction of the total sulfate aerosol mass concentration that is included in cloud droplets during the nucleation scavenging is ~0.7-0.9 [*Hobbs*, 1993], and we use a fixed value of 0.8 in the runs presented here.

The removal of SO_2 and $SO_4^{(2-)}$ by precipitation is described using the fluxes of water in the form of q_s and q_r. Fluxes of sulfur between various forms of water are calculated in the same manner. For instance, if $F(q_c \rightarrow q_r)$ is the flux of water from cloud droplets into rain droplets, then the flux of sulfur from cloud droplets into rain droplets is given by $F(q_{scw} \rightarrow q_{sr}) = F(q_c \rightarrow q_r) \times q_{scw}/q_c$. The module described here allows

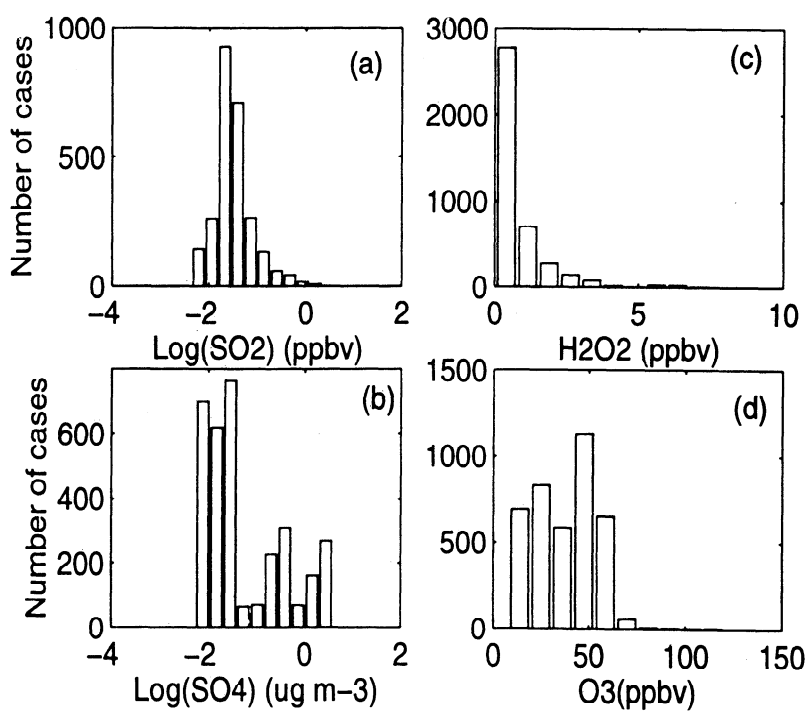

Figure 3. Histograms of (a) SO_2 (ppbv), (b) $SO_4^{(2-)}$ ($\mu g\ m^{-3}$), (c) H_2O_2 (ppbv), and (d) O_3 (ppbv) in western Pacific as deduced from PEM-West B.

the estimation of the total sulfate concentration in a convective field, based on initial conditions of SO_2 and aerosol sulfate, $SO_4^{(2-)}$, concentrations. This module is used to evaluate the effects of convection on sulfur species, as well as to provide the distribution of dry sulfate concentration at the cloud base required for the CCN-sulfate relationship as described in section 2.3.

2.3. CCN-Sulfate Relationship

There is considerable experimental evidence that the CCN concentration increases with the sulfate concentration [*Leaitch et al.*, 1992; *Quinn et al.*, 1993; *Leaitch and Isaac*, 1994; *Hegg et al.*, 1993, 1994; *Boucher and Rodhe*, 1994; *Van Dingenen et al.*, 1995]. The physical causes of this relationship are the following: (1) An increase of $SO_4^{(2-)}$ concentration is associated with emissions of SO_2 and condensation nuclei (CN), both from natural and anthropogenic sources; SO_2 is also an efficient source of $SO_4^{(2-)}$ by creating new CN especially in the free troposphere (FT); some of these new particles grow and become CCN. (2) An increase of SO_2 concentration produces more sulfate by oxidation, and this sulfate accumulates on preexisting aerosol increasing their size. This enables more CN to become CCN [*Pandis et al.*, 1994; *Hobbs*, 1993; *Hegg et al.*, 1996].

A common relationship between the cloud droplet concentration, N_d, and the sulfate concentration in liquid drops, q_{scw} in units of μg m^{-3}, has the form $\log_{10}(N_d)=a+b\times\log_{10}(q_{scw})$, where a and b are empirical constants that can be determined from measurements [see e.g., *Van Dingenen*, 1995]. Such nonlinear relationship has a square of the Pearson-r correlation coefficient ~0.5-0.7 and was used extensively for the estimations of the indirect effects of sulfate aerosols with GCMs [*Boucher and Lohmann*, 1995]. However, as pointed out by *Chuang and Penner* [1995], the characteristics of the cloud droplet size distribution near the cloud base are dependent on the aerosol properties below the cloud base and on the local updraft velocities. Following their approach, we use the dry sulfate concentration, q_{ds}, predicted by the model and assume a lognormal size distribution with parameters $\bar{D}$=0.1 μm and geometric standard deviation σ_g=2.0 to derive the total number concentration of aerosol at the cloud base N_a [*Kiehl and Briegleb*, 1993]. The concentration of cloud droplets at the cloud base can be expressed as a function of updraft velocity, w, and the total number concentration of aerosol, N_a, in the form $N_d=wN_a/(wN_a+cN_a)$, where c is a scaling parameter designed such that the predicted N_d matches the simulated values from a microphysical model [see *Ghan et al.*, 1993; *Chuang and Penner*, 1995; *Chuang et al.*, 1997]. After the formation of cloud droplets, the growth by collection tends to reduce their number concentration. The gravitational collection (due to differences in the terminal velocities) dominates over the brownian collection for the typical drop sizes in natural clouds, and the decrease of N_d in time can be approximated by

$$N_d(t) = N_d(0)[1 - \frac{2.55 \times 10^5 q_c^{4/3} t}{N_d(0)^{1/3}}] \quad (4)$$

where $N_d(0)$ is the cloud droplet concentration at cloud base (in cm^{-3}), q_c is the liquid water content (in g cm^{-3}), and t is time in seconds. Since during the updraft, $dz=w\times dt$, the relation given above can be used to diagnose the vertical distribution of the total number concentration of cloud droplets [see *Pruppacher and Klett*, 1978].

2.4. Initial and Boundary Conditions

The model was integrated to simulate a 6-day TOGA COARE case, from December 20-25, 1992, in a domain centered at (2°S, 156°E), with a time step of 2 s. The choice of this case is based on well-defined intense convective activity in the area of interest [*Lin and Johnson*, 1996; *Short et al.*, 1997; *Moncrieff et al.*, 1997; *Godfrey et al.*, 1998]. The LAN model is a cloud resolving model with governing equations that include large-scale forcing terms. These large-scale forcing terms are approximately uniform over the model domain, which is small compared to the large-scale disturbances. The model was initialized with large-scale area average profiles of observed temperature, water mixing ratio, and horizontal velocity components. The initial sounding from December 20, 1992, t=0 hour UT, is shown in Figure 4. Figure 4 shows the potential temperature (solid line), θ, and the equivalent potential temperature of a hypothetically saturated atmosphere which has the thermal structure of the actual atmosphere (crosses) θ_e^* [*Holton*, 1979]. The derivative $\partial\theta_e^*/\partial z$ provides a rapid indication of the conditional stability of a saturated air parcel. In the case from Figure 4a, for $z < 3$ km, $\partial\theta_e^*/\partial z < 0$, and the air is conditionally unstable. The wind profiles indicate westerlies near the surface and easterlies in the mid troposphere and upper troposphere and predominant southward flow (Figure 4b).

The large-scale forcing terms are defined as functions of height and time and are based on observations over the intensive flux array (IFA) region, which extends about 500 km [*Webster and Lukas*, 1992]. The large-scale forcing treatment in this study follows the one described by *Moncrieff et al.* [1997] and includes the large-scale advective tendencies of potential temperature, $(\partial\bar{\theta}/\partial t)_{L.S}$, water mixing ratio, $(\partial\bar{q}/\partial t)_{L.S}$, and the horizontal momentum, $(d\bar{v}/dt)_{L.S}$. The large-scale advective tendencies for potential temperature, θ, and water mixing ratio, q, are

$$(\frac{\partial\bar{\theta}}{\partial t})_{L.S} \equiv -\bar{v}\nabla\bar{\theta} - \bar{w}\frac{\partial\bar{\theta}}{\partial z} \quad (5)$$

$$(\frac{\partial\bar{q}}{\partial t})_{L.S} \equiv -\bar{v}\nabla\bar{q} - \bar{w}\frac{\partial\bar{q}}{\partial z} \quad (6)$$

available at 6-hour intervals. These values are interpolated in height to the model's grid and in time to obtain values at each time step. The large-scale forcing term

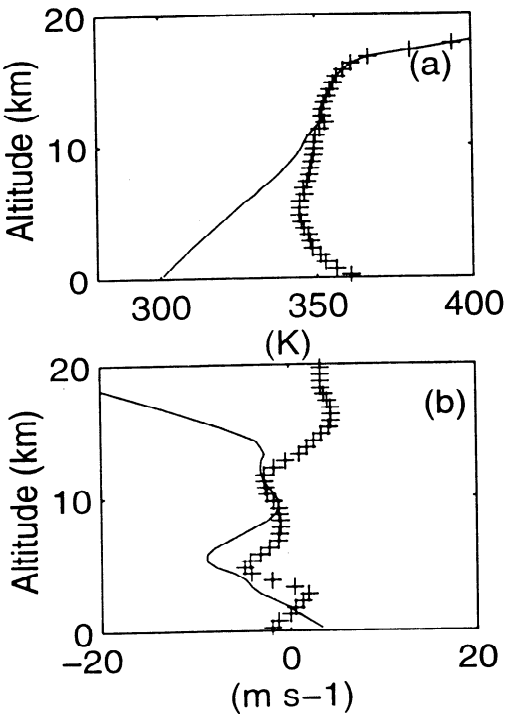

Figure 4. Initial vertical sounding from TOGA COARE, December 20, t=0 hour UT from 2°S-156°E, used to initialize the cloud resolving model: (a) potential temperature (solid line) and equivalent potential temperature (crosses) and (b) zonal wind component U (solid line) and meridional wind component V (crosses).

in the horizontal momentum equation is given by

$$\left(\frac{d\bar{\mathbf{v}}}{\partial t}\right)_{\text{L.S}} = -\frac{\bar{\mathbf{v}} - \bar{\mathbf{v}}_{\text{obs}}}{\tau} \qquad (7)$$

where $\bar{\mathbf{v}}$ is the predicted large-scale horizontal velocity, $\bar{\mathbf{v}}_{\text{obs}}$ is the observed large scale velocity, and τ is an adjustment time (τ=7200 s) [*Moncrieff et al.*, 1997; *Wu et al.*, 1998]. By using this procedure, the predicted horizontal wind does not depart too much from observations.

The lower boundary of the model is an ocean surface, and its properties are specified by surface pressure and sea surface temperature (SST). The observed values at 6-hour intervals are interpolated to obtain values at each time step. Periodic lateral boundary conditions were applied for all dynamic variables, and a sponge-type condition was applied at the top of the model domain to attenuate the gravity waves induced by convection. The convection is initiated by applying small random perturbations in the potential temperature in the boundary layer (BL). This procedure was applied successfully by *Haywood et al.* [1997] and *Donner et al.* [1998], producing realistic physical fields for a convective system in a tropical area. Once the convective cells are formed, their evolution is controlled by the internal dynamics of the model and by the large-scale forcing.

Measurements of SO_2 and $SO_4^{(2-)}$ are not available during the TOGA COARE experiment. Vertical profiles of SO_2 and $SO_4^{(2-)}$ from the PEM-West B, based on the observations during DC-8 aircraft flights over the tropical regions of the western Pacific during February-March 1994, were used to initialize the variables of the sulfate module [*Hoell et al.*, 1997; *Talbot et al.*, 1997]. This choice is based on the assumption that the emissions and distributions of sulfur species measured during PEM-West B are representative over the area of interest.

3. Results and Discussion

3.1. Sulfur in Tropical Pacific Atmosphere

Recent measurements and modeling studies indicate that sulfur species in the western Pacific atmosphere originate from sea salts, dymethylsulfide (DMS), volcanic emissions, and anthropogenic sources [*Chin and Jacob*, 1996; *Thornton et al.*, 1997a, b; *Xiao et al.*, 1997]. The Pacific Exploratory Missions West (PEM-West) of NASA, during September-October 1991 (phase A) and February-March 1994 (phase B), provided the opportunity to measure sulfur species such as SO_2, DMS, and $SO^{(2-)}$, as well as tracers and chemical species that could be used to characterize and identify various sources of sulfur [*Thornton et al.*, 1997a, b; *Talbot et al.*, 1997]. On the basis of the analysis of these data, it was found that the SO_2 concentration is impacted by (1) DMS oxidation in the BL, as well as in the free and upper troposphere, (2) long-range transport from continental sources (biogenic and anthropogenic), and (3) volcanic emissions in the western Pacific regions [*Xiao et al., 1997*; *Thornton et al.*, 1997a, b].

During the phase A of PEM-West (September-October 1991), the SO_2 was found strongly perturbed by the Mount Pinatubo eruption (June 1991). In contrast, during the phase B of PEM-West (February-March 1994), the effects of Pinatubo were much smaller, and the continental outflow from Asia was favored by the intense winter eastward circulation. In this sense, PEM-West B illustrates better the impact of Asian continent outflow on the western Pacific, as documented by tracers such as lead-210, and C_2H_2/CO ratios [*Thornton et al.*, 1997b]. While the impact of the outflow on the Pacific atmosphere was the strongest at midlatitudes, because of the rapid passage of cold fronts during the winter, episodic increases in SO_2 and $SO_4^{(2-)}$ were also documented for the tropical western Pacific. A compilation of the data taken during flights from the tropical area from PEM-West B are given in Figure 3 as histograms of the number of cases of SO_2 and $SO_4^{(2-)}$ for various concentration intervals (shown in logarithmic scale). Most of the samples are from FT and upper troposphere, where the SO_2 concentration is well below 0.1 ppbv. In BL flights SO_2 was found ~0.1-1.0 ppbv and occasionally higher. $SO_4^{(2-)}$ concentrations are also small in the upper troposphere (less than ~0.1 μg m^{-3}), but there are many cases in which it exceeds 1 μg m^{-3} in the BL. The vertical distribution of SO_2 and $SO_4^{(2-)}$

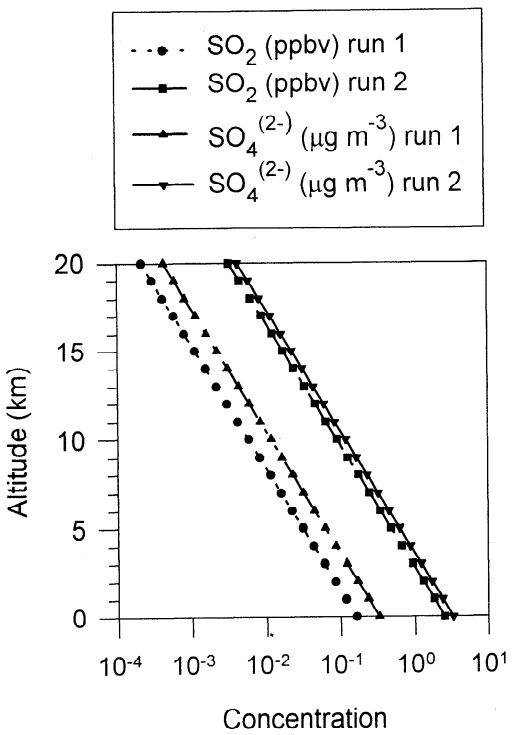

Figure 5. Vertical profiles of SO_2 and $SO_4^{(2-)}$ concentrations in tropical western Pacific as deduced from PEM-West B and used to initialize the model.

concentrations observed during PEM-West B are used to generate initial and boundary conditions for the sulfur distribution used in this study. The minimum values of SO_2 and $SO_4^{(2-)}$ concentrations measured are typical for a clean remote atmosphere and are used in run 1, while the maximum concentrations are more typical for significant perturbations (most likely anthropogenic and volcanic) and are used in run 2. These values were fitted exponentially and the resulting curves are given in Figure 5, resulting in two scenarios of low- and high-atmospheric sulfur loading. The use of these profiles in our calculations enable us to assess the effect of an increase of SO_2 and $SO_4^{(2-)}$ on the tropical Pacific convective cloud systems.

3.2. Convective Activity in the Tropical Pacific

The western Pacific warm pool, a domain delimited roughly by 10°S-10°N and 140°E date line, is the region with the warmest SST in the open ocean and the largest annual rainfall and latent heat release in the atmosphere [*Webster and Lukas*, 1992]. Tropical convective systems in this area play an important role in the global redistribution of heat, moisture and momentum. The TOGA COARE experiment was designed to study the role of the western Pacific warm pool in the mean and transient state of the tropical ocean-atmosphere system. Analysis of the satellite and meteorological data indicate that the TOGA COARE area experiences several specific phenomena that affect cloudiness and rainfall: (1) an annual cycle, (2) an intraseasonal oscillation (ISO), or the Madden-Julian Oscillation, with a 40-60 day period, and (3) occasional westerly wind bursts. For details of the experiment design, characteristics of the atmospheric circulation and precipitation measurements during the intense observation period (IOP) see *Webster and Lukas* [1992], *Lin and Johnson* [1996], and *Short et al.* [1997].

The case used in the present study is based on the measurements taken during December 20-25, 1992, which was characterized by convective events. These events were associated with a major ISO and the passage of a major supercluster, strong westerly winds at the surface, and easterly winds aloft. An example of convective activity is illustrated in Figure 6, which shows an instantaneous spatial distribution of model simulated liquid and ice cloud water concentration, rain water concentration, and total cloud water (including liquid, ice, snow and rain) at t=12 hours UT of December 20, 1992, in a domain centered at 2°S-156°E, corresponding to a snapshot of model results after 12 simulated hours. Figure 6a shows the presence of two convective towers, with q_c reaching values of ~0.5 g kg^{-1} in the core as well as in the upper troposphere, where large anvils are present. Observations indicated the presence of extensive optically thick anvil clouds and nonprecipitating high cirrus [*Lin and Johnson*, 1996]. Figure 6b shows typical spatial distribution of rain, with intense q_r~0.5 g kg^{-1} over few kilometers, separated by domains of lower rain or no precipitation. Figure 6c indicates that the maximum of total condensed water in the two convective towers reaches ~1 g kg^{-1}, between 2 and 8 km altitude. This configuration corresponds to an average unstable equivalent potential temperature (Figure 7a), westerlies in the lower troposphere and easterlies in the rest of troposphere, and mostly southward motions (Figure 7b), large-scale cooling in the FT, and large-scale horizontal convergence of specific humidity (Figure 7c).

The case of IOP studied here produced an example of the quasi 2-day oscillation clearly observed in the radar time series [*Short et al.*, 1997], as well as in the vertical profiles. Figure 8 represents the time evolution of the model-simulated horizontal average of the cloud water concentration (liquid and ice) (plot starts at t=0 hours UT, December 20, 1992), rain water concentration, and total cloud condensed water. Figure 8a shows intense average convective activity during the 6-day period, with three intervals of lower q_c concentrations in the time intervals 36-60 hours, 72-96 hours, and 132-144 hours. The rain patterns (Figure 8b) and the total condensed water concentration (Figure 8c), confirm this time distribution, supported by the observations of the quasi 2-day oscillation caused by the large-scale forcing [*Lin and Johnson*, 1996; *Moncrieff et al.*, 1997]. The large-scale conditions were dominated by westerlies in the lower troposphere and easterlies in the free and upper troposphere (Figure 9a), southward motions in the

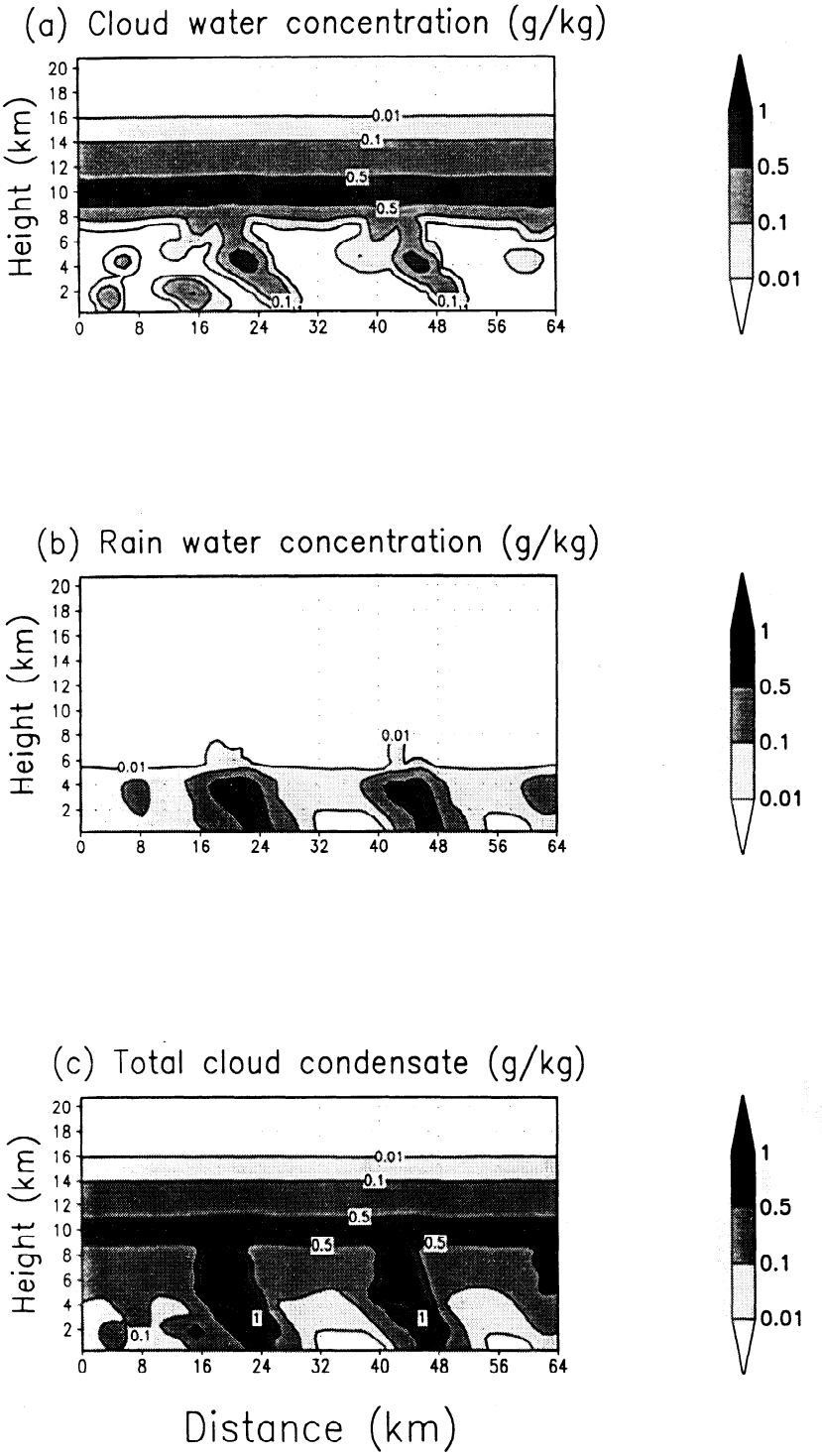

Figure 6. Instantaneous spatial distribution of model simulated (a) liquid and ice water concentration, q_c, (b) rain water concentration, q_r, and (c) total cloud water (including liquid, ice, snow, and rain), at t=12 hours UT of December 20, 1992, in a domain centered at 2°S-156°E. (The snapshot corresponds to the model results after 12 simulated hours.)

free troposphere, intense northward motions around 14 km (Figure 9b), and relative humidity (with respect to liquid water) favorable for cloud formation (Figure 9c). Figure 10 compares the rates of rainfall as observed [*Short et al.*, 1997] and estimated by our model. While discrepancies exist, our model captures the main features of the precipitation pattern and is in good qualitative agreement with observations.

3.3. Effect of Convection on Sulfur

Convective transport is very effective in transporting sulfur species in the troposphere [*Chatfield and Crutzen*,

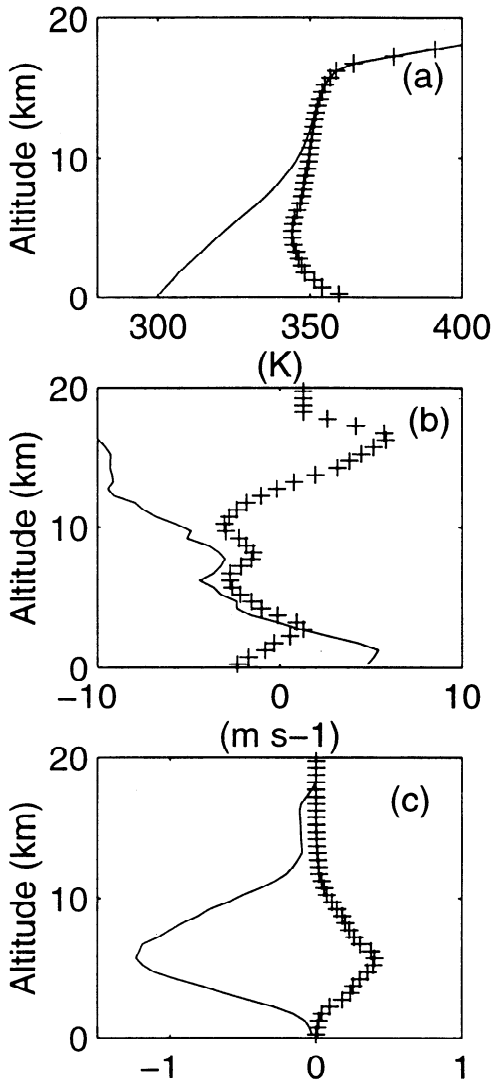

Figure 7. Vertical sounding from TOGA COARE, December 20, t=12 hours UT from 2°S-156°E, corresponding to the example given in Figure 6: (a) potential temperature (solid line) and equivalent potential temperature (crosses), (b) zonal wind component U (solid line) and meridional wind component V (crosses), and (c) large-scale tendency of potential temperature (K hour^{-1}) (solid line) and the large-scale tendency of specific humidity (g kg^{-1} hour^{-1}) (crosses).

1984; *Flossmann*, 1991; *Wang and Chang*, 1993; *Wang et al.*, 1995; *Taylor et al.*, 1997; *Kreidenweis et al.*, 1997]. The average profiles of SO_2 and $SO_4^{(2-)}$ concentrations are used to initialize the model in order to illustrate the effect of convective transport on the redistribution of these species. The presence of clouds has a dramatic impact on sulfur species not only by direct transport but also because of effective scavenging of $SO_4^{(2-)}$ particles during the nucleation process and rapid in-cloud oxidation of SO_2 in cloud droplets.

Figure 11 shows an example of instantaneous spatial distribution of concentrations of SO_2 in gas phase, $SO_4^{(2-)}$ in particulate phase, and as total sulfate in aqueous phase, at t=12 hours UT, December 20, 1992, as simulated with our model, using conditions from the "clean" scenario described as run 1 in Figure 5. Figure 11a shows that SO_2 concentration decays with altitude and has levels of ~20 parts per trillion by volume (pptv) in upper troposphere and considerable depletion in the region of high-liquid content, between about 3 and 6 km. In this layer, SO_2 is converted to aqueous $SO_4^{(2-)}$. In contrast to the SO_2 concentration, the $SO_4^{(2-)}$ particulates are very efficiently scavenged by clouds, becoming negligible above about 6 km altitude in updrafts, and above the BL in downdrafts (Figure 11b). This decay of particulate $SO_4^{(2-)}$ concentration is caused by the nucleation scavenging, which converts it to aqueous sulfate. Figure 11c shows the distribution of aqueous $SO_4^{(2-)}$ concentration with maximum values above 100 ng kg^{-1} in the cores of convective towers.

Figures 12a, 12b, and 12c show examples of horizontal averaged vertical profiles of SO_2 in gas phase, $SO_4^{(2-)}$ in particulate phase, and as total sulfate in aqueous phase with the standard deviations for December 20, t=12 hours UT. In the case of SO_2, the average concentration at the surface is ~100 pptv and drops to ~10-20% of this value in the FT and upper troposphere. The concentration of $SO_4^{(2-)}$ in particulate phase has a value of ~200 ng kg^{-1} near the surface and decays to about 10% in FT and upper troposphere. Over the same height range, the concentration of aqueous $SO_4^{(2-)}$ increases in the layer 2-4 km, where the highest concentration of liquid cloud water is found. The behavior described here for the SO_2 and $SO_4^{(2-)}$ concentrations is quite similar with results described by *Wang and Crutzen* [1995] based on simulations of a severe storm.

3.4. Effect of Sulfate on Convective Clouds

To estimate the effect of sulfate on the convective clouds as simulated with the LAN model, we choose to compare two runs that correspond to the minimum (run 1) and maximum (run 2) observed values of SO_2 and $SO_4^{(2-)}$ concentrations during PEM-West B in the tropical area (see Figure 5). The minimum sulfate is more typical for a clean, remote atmospheric region, while the maximum sulfate case is more typical for polluted scenarios [*Thornton et al.*, 1997b; *Talbot et al.*, 1997]. Previous work suggested that a change in sulfate aerosol loading can produce noticeable changes in cloud microphysics. In situ measurements reported by *Pruppacher* [1981] and recent retrieval of cloud particle radii from satellite data available from the International Satellite Cloud Climatology Project show that cloud droplet radii in continental clouds are smaller than those in marine clouds [*Han et al.*, 1994]. Since $r_e \sim (q_c/N_d)^{1/3}$, it is possible that a change in sulfate loading increases N_d and reduces r_e, an aspect that is explored in section 3.4.1.

3.4.1. Effects of sulfate on microphysics. The effects of sulfate on the effective radius and number con-

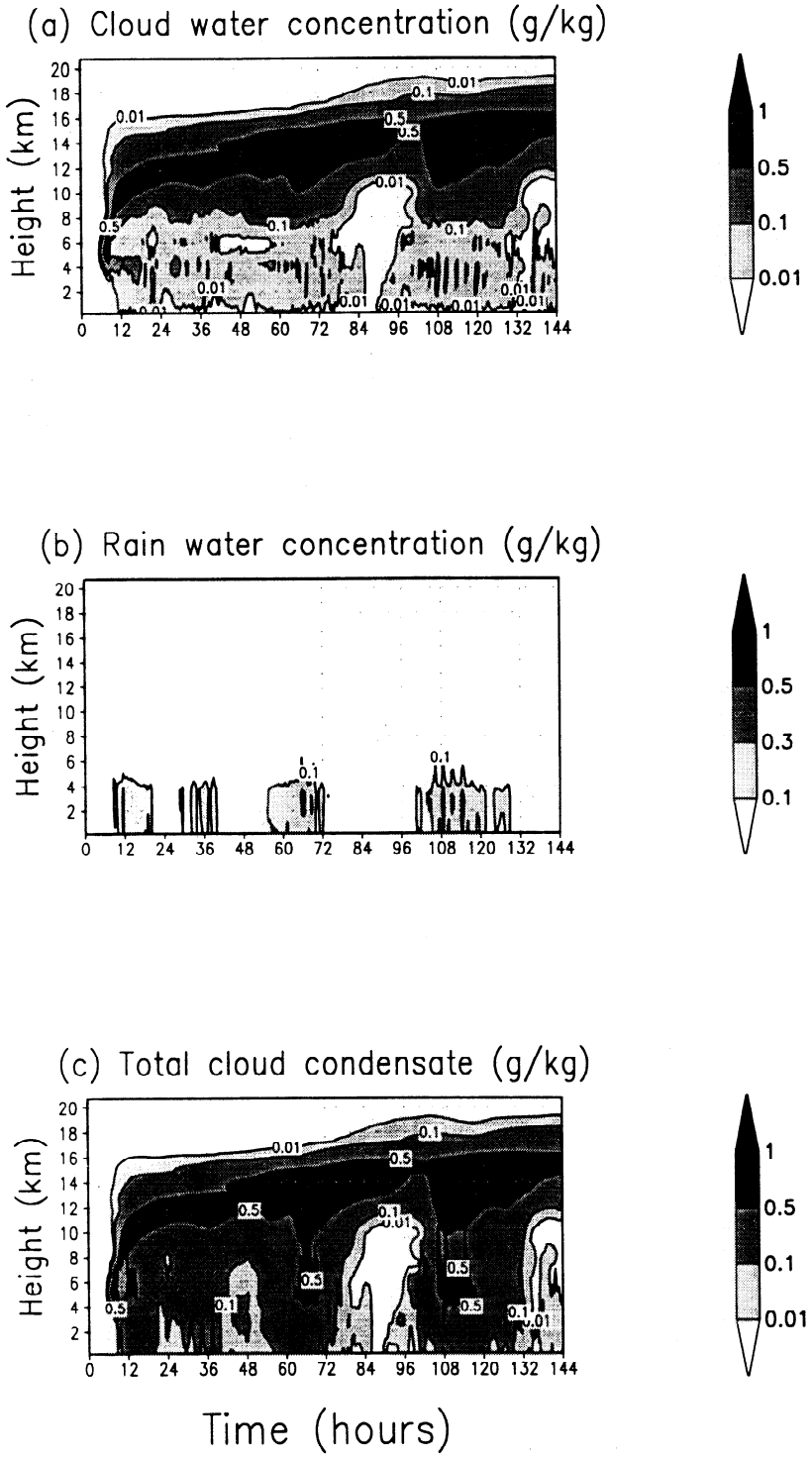

Figure 8. Time evolution of the horizontal average of (a) cloud water concentration (liquid and ice), (b) rain water concentration, and (c) total condensed cloud water for the interval December 20-25, 1992.

centration of cloud droplets are illustrated in Figure 13. For Figure 13 we used average parameters from time intervals with negligible rain (q_r<0.1 g kg^{-1}) during the 6-day period. Figure 13a shows the histogram of r_e for run 2 indicating sizes roughly between 2 and 20 μm, with most frequent sizes between 5 and 10 μm, an average of 9.6 μm, and a standard deviation of 4.6 μm. The changes in r_e between the two runs are shown in Figure 13b. There is an increase up to 2 μm in r_e when the aerosol is decreased from run 2 to run 1. The average change is 0.9 μm, and the standard deviation is 0.5 μm. Qualitatively, this compares well with the results reported by *Han et al.* [1994] based on the satellite data, where they found r_e~3-30 μm, with an average of

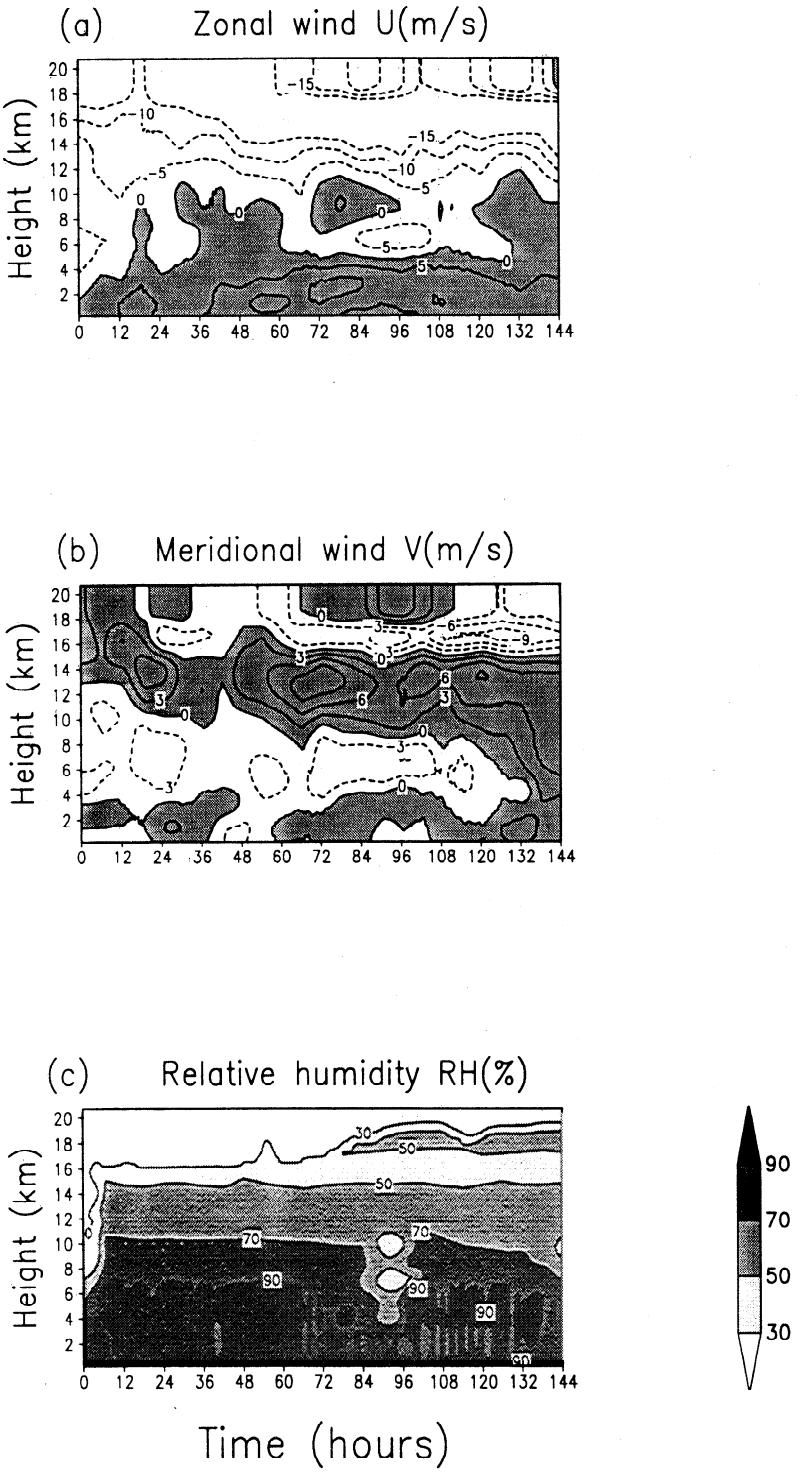

Figure 9. Time evolution of the horizontal average of (a) zonal wind U (shaded areas indicate westerlies), (b) meridional wind V (shaded areas indicate northward flow), and (c) relative humidity with respect to liquid water, for the interval December 20-25, 1992.

~10 μm. For instance, they found that cloud droplets in continental water clouds are ~2-3 μm smaller than in marine clouds. Considering that run 1 is typical for a clean marine scenario and run 2 is somehow impacted by sulfate transport, typical for continentally influenced conditions, the comparison indicates good agreement between available observations and our simulations. We note that both in our model and the results given by Han et al. the effect of ice particles is not included. We assumed here only spherical droplets which freeze and are lifted by convection in the upper troposphere, where they eventually persist in anvils or cirrus clouds. We found that for the changes in aerosol at cloud base between run 1 and run 2 there is very little impact on

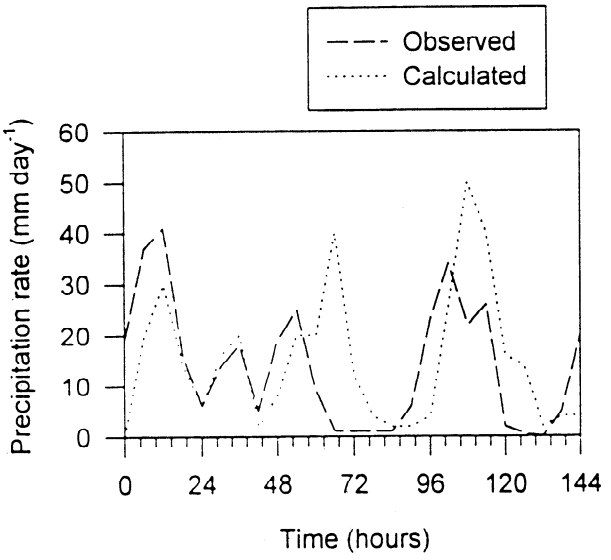

Figure 10. Simulated and observed rainfall rates. Observations are based on the work by *Short et al.* [1997].

the r_e and N_d in the upper troposphere due to rapid decay with altitude of N_d perturbations.

Figure 13c shows the histogram of N_d for the case of run 2, indicating number cloud concentrations ~20-100 cm^{-3}, with most frequent values less than 50 cm^{-3} an average of 47 cm^{-3}, and a standard deviation of 21 cm^{-3}. The changes in N_d between run 1 and run 2 are between 0 and ~40 cm^{-3}, with most frequent changes below ~15 cm^{-3} (Figure 13d). The average change was found equal with 16 cm^{-3} with a standard deviation of 12 cm^{-3}. Observations reported by *Dong et al.* [1997] indicate values of N_d~ 150 cm^{-3} in marine clouds (in the Azores), a value close to our estimate for high sulfate. The relationship between CCN and N_d was pointed out by other previous experimental work [*Hobbs*, 1993], and it is reasonable to assume that a change in sulfate loading, as shown in the distribution of sulfate at cloud base, can produce variations in CCN, N_d, and r_e. More dramatic changes were shown by *Ackerman et al.* [1995], who documented changes in cloud r_e and N_d induced by ship tracks. They found changes in r_e of ~4 μm and changes in N_d of ~80 cm^{-3} between ambient clouds and clouds affected by ship emissions. Our results show significantly smaller changes due to the less intense aerosol perturbation assumed here. Thus the increase of sulfate has the potential to alter the number concentration of CCN able to grow as cloud droplets, and the effect on N_d and r_e is quite significant for the tropical convective clouds and is in reasonable agreement with the available observations. Such changes in cloud parameters have an impact on the radiative-flux distribution and particularly on the shortwave radiative flux above the cloudy domain.

3.4.2. Effects of sulfate on radiative fluxes. Fluxes of shortwave (SW) and longwave (LW) radiation are calculated for each grid point. Each flux has an upward (up) and a downward (dn) component. We define $SW_{net}=SW_{dn}-SW_{up}$, the net SW radiation flux, and $LW_{net}=LW_{dn}-LW_{up}$, the net LW radiation flux. To obtain a more robust characterization for the entire convective domain, we produce horizontal averages of these fluxes. Changes in radiative fluxes caused by sulfate can be estimated by calculating differences between the case with maximum (run 2) and minimum (run 1) sulfate concentrations.

The SW radiative flux is dependent upon cloud particle size and CWP in the radiative code used in our model. Thus it appears that changes induced by aerosols in both CWP and particle size can be responsible for the variations of SW above clouds. The impacts of cloud droplet size and CWP on the SW flux can be illustrated by considering the dependence of the cloud optical depth, τ, on CWP and r_e, for a given spectral interval [*Slingo*, 1989]

$$\tau = \mathrm{CWP}(a + \frac{b}{r_e}) \tag{8}$$

where a and b are constants for a given spectral interval and their typical values are a ~10^{-2} m^{2}g^{-1} and b ~1 μm m^{2}g^{-1}. The relation (4) can be written as $\ln(\tau)=\ln(\mathrm{CWP})+\ln(a+b/r_e)$, which by differentiation and considering r_e~10 μm gives the relative changes in τ as a function of relative changes in CWP and r_e

$$\frac{\delta\tau}{\tau} \approx \frac{\delta(\mathrm{CWP})}{\mathrm{CWP}} - \frac{\delta r_e}{r_e} \tag{9}$$

Time variations of $\delta(SW_{net})=SW_{net}$(run 2)-$SW_{net}$(run 1), at 20 km altitude and horizontally averaged, are shown in Figure 14a. We note that an increase of aerosol from minimum to maximum observed values in the PEM-West B produces a decrease of SW_{net} above clouds as much as -3 W m^{-2} and a time average of $\delta(SW_{net})$ of -1.5 W m^{-2} over the daylight intervals and a standard deviation of 1.4 W m^{-2}. This effect is caused by the increase of the optical depth due to changes in CWP and the average effective radius of cloud droplets. Time variations of domain-averaged relative changes in effective radius, $\delta r_e/r_e$ for the column average of r_e, and δ(CWP)/CWP are shown in Figures 14b and 14c. The relative change of the effective radius is mainly between -10 and -30%, with a time and vertical average of -18.0% (Figures 14b). Because $\delta r_e/r_e<0$ when aerosol loading increases, the effect of this term is to increase the optical depth and cloud reflectivity. In contrast, the relative variations of CWP can be of both signs, and these changes are roughly between -30 and 30% (with typical absolute values <10%) (Figures 14c). We note that $\delta r_e/r_e$ correlates positively with δ(CWP)/CWP (Figure 15a), and the smallest values of δ(CWP)/CWP are about -30% while $\delta r_e/r_e$ values are -30 to -40%. Therefore, for the case simulated here, $\delta\tau/\tau>0$, leading to a negative change in SW_{net} above clouds during the day in most cases. This can be further illustrated by the scatterplot of $\delta(SW_{net})$ versus δ(CWP)/CWP in

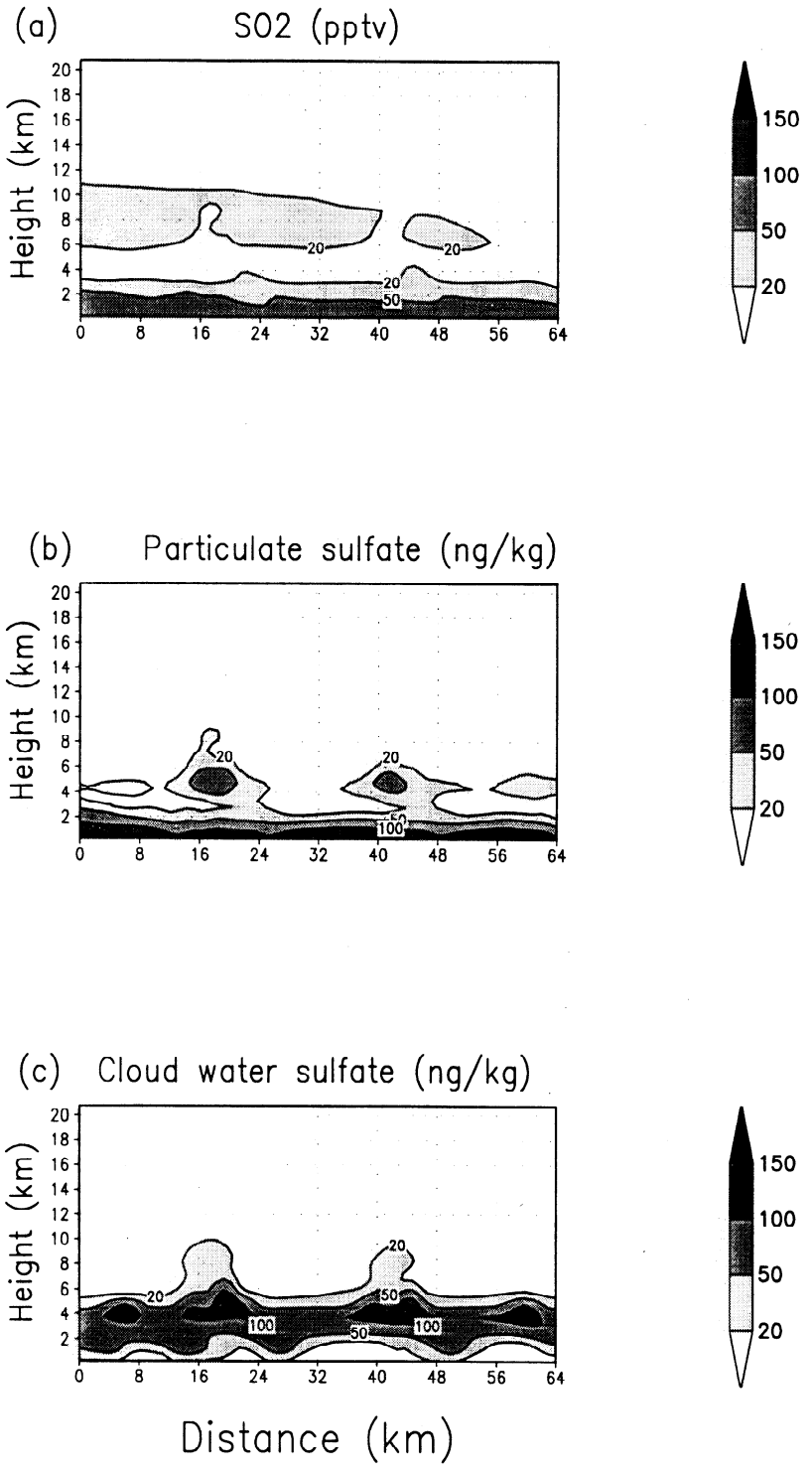

Figure 11. Example of instantaneous space distribution of (a) SO_2 concentration, (b) particulate sulfate, and (c) cloud water sulfate concentration at t=12 hours UT, December 20, 1992.

Figure 15b. This plot shows that more SW radiation is reflected by clouds in instances with higher CWP that are connected with thicker clouds or an increase of q_c. While correlations shown here are not strong, they suggest that both the cloud particle size and CWP variations induced by aerosols are controlling the local changes of the SW radiation flux above clouds.

Figure 16a shows the time variation of the horizontal average of $\delta(LW_{net})=LW_{net}(run2)-LW_{net}(run1)$ near the surface for the 6 simulated days. We note variations of $\delta(LW_{net})$, with values as much as 10 W m^{-2} or higher in absolute magnitude, but with a time average of only 0.5 W m^{-2} (and a large temporal variability indicated by the standard deviation of 5.4 W

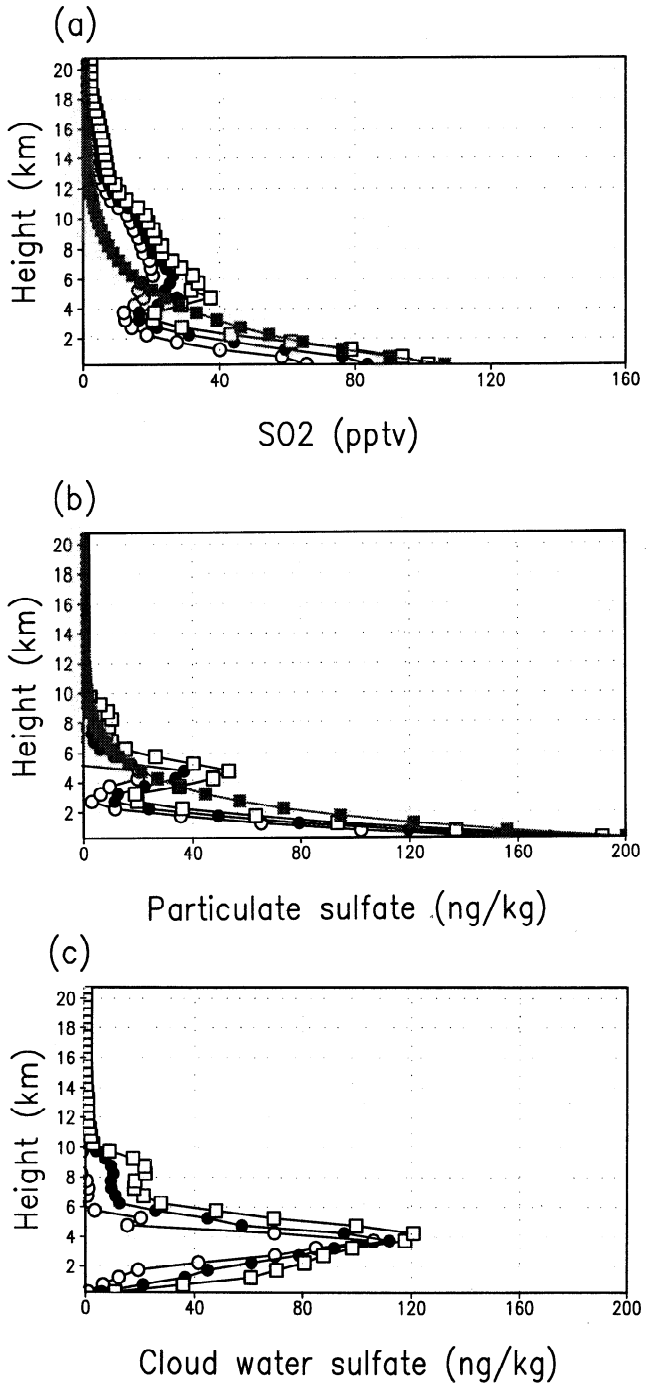

Figure 12. Simulated horizontal average of (a) SO_2 concentration, (b) particulate sulfate, and (c) cloud water sulfate concentration, for December 20, 1992, t=12 hours UT. The average profile (filled circles), average plus one standard deviation (open squares), and average minus one standard deviation (open circles) are shown. The initial profiles for SO_2 and dry sulfate are shown for comparison (gray squares).

m^{-2}), suggesting that over longer time periods the time average of $\delta(LW_{net})$ is negligible. The vertical distribution of $\delta(LW_{net})$ in the integration domain was found to exhibit variations as high as those close to the surface, but, above clouds, the changes are negligible. We investigated whether these changes in $\delta(LW_{net})$ are somehow connected with changes in air temperature and in CWP. The changes in $\delta(LW_{net})$ are accompanied by changes in the air temperature field, but we found no significant correlation between the two fields. The changes in air temperature near the surface, caused by the aerosol difference, are generally between -1°C and 1°C (significantly smaller than the variations observed during TOGA COARE, where near the surface, the air temperature had observed variations of ~5°C), and they do not appear to correlate with $\delta(LW_{net})$ over all the integration time interval. However, such changes in temperature might become significant in instances of polluted scenarios, since we found that they tend to increase if the sulfate concentration is enhanced.

We turn now to search for a possible link between the changes in $\delta(LW_{net})$ near the surface and the variations in cloud water distribution caused by aerosol increase. Owing to changes in the radiative fields, there is a feedback on the model dynamics that produces changes in variables that in turn affect the LW flux. This is illustrated by Figure 16b, which gives a scatterplot of the surface $\delta(LW_{net})$ with $\delta(CWP)/CWP$ and shows a slight positive correlation, indicating that an increase in CWP tends to increase the $\delta(LW_{net})$ near the surface. This can be further illustrated in Figure 17, which shows changes in the q_c when the aerosol is increased from the minimum to the maximum observed values during PEM-West B experiment (similar changes were found in other cloud variables). We note that these changes are typically of the order of 0.01 g kg^{-1}, generally much smaller than the typical absolute values of q_c for example, which is of the order of 0.1 to 1 g kg^{-1} (shown by the solid lines in Figure 17), and there are no large changes in the regions of upper troposphere where the ice clouds dominate.

Thus it appears that for realistic variations of sulfate concentration, consistent with the observed values during PEM-West B over the tropical region simulated here, the net time average changes in temperature and CWP are negligible in comparison with the "natural variations" of these parameters, as observed during the TOGA COARE experiment. In the view of the simulations and results presented here, the main effect of realistic sulfate increase in tropical convective domains in the TOGA COARE region is a slight increase of SW cloud albedo. These model results provide the spatially and temporally detailed variations of these changes, as well as an indication that they are linked to variations in cloud microphysical parameters and cloud water distribution in the convective system.

4. Conclusions

A two-dimensional version of the GFDL LAN model with an explicit sulfate-cloud microphysics scheme was applied to a TOGA COARE case of tropical convective event. The model was forced by observed sound-

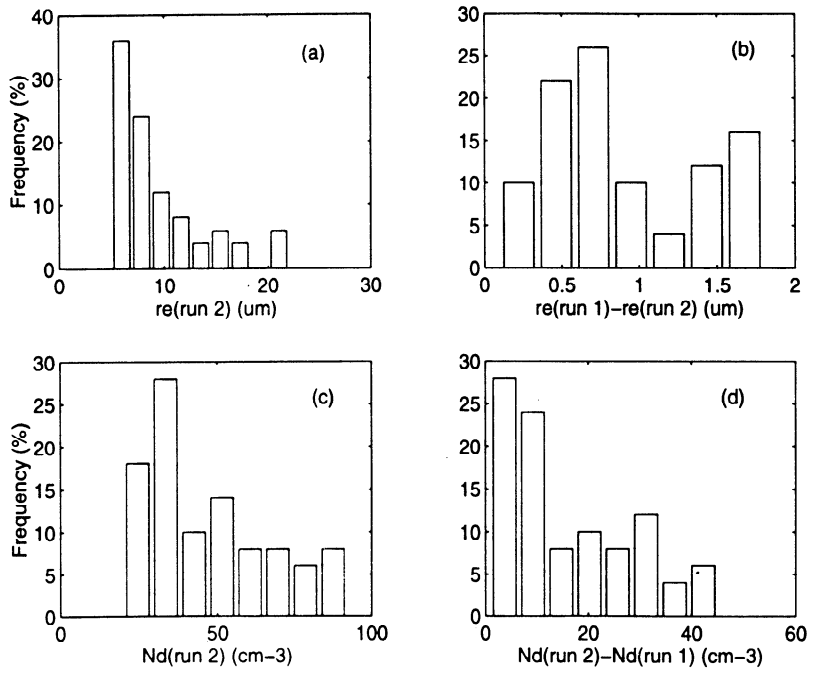

Figure 13. Frequency of cases with (a) effective radius of cloud droplets, r_e, in the indicated interval, for run 2; (b) changes in r_e between run 1 and run 2; (c) N_d for run 2, and (d) changes in N_d from run 1 to run 2. Data used in these histograms are from time intervals with absent or negligible rain.

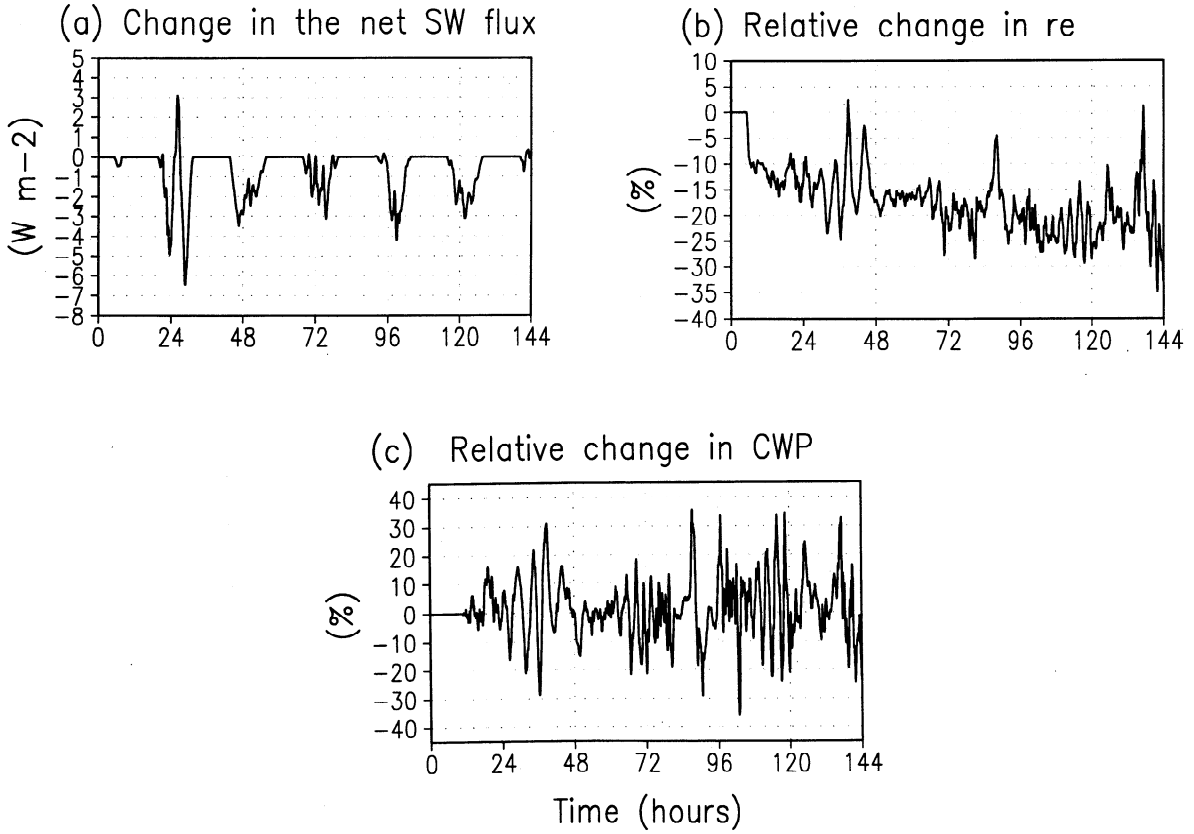

Figure 14. (a) Time evolution of the calculated horizontal average change in the net shortwave radiative flux, $\delta(\mathrm{SW_{net}})$ (W m^{-2}), above the cloudy domain (z=20 km), (b) relative change of the vertical and horizontal average of r_e (percent), and (c) relative change of the horizontal average of CWP (percent), for the time interval December 20-25, 1992.

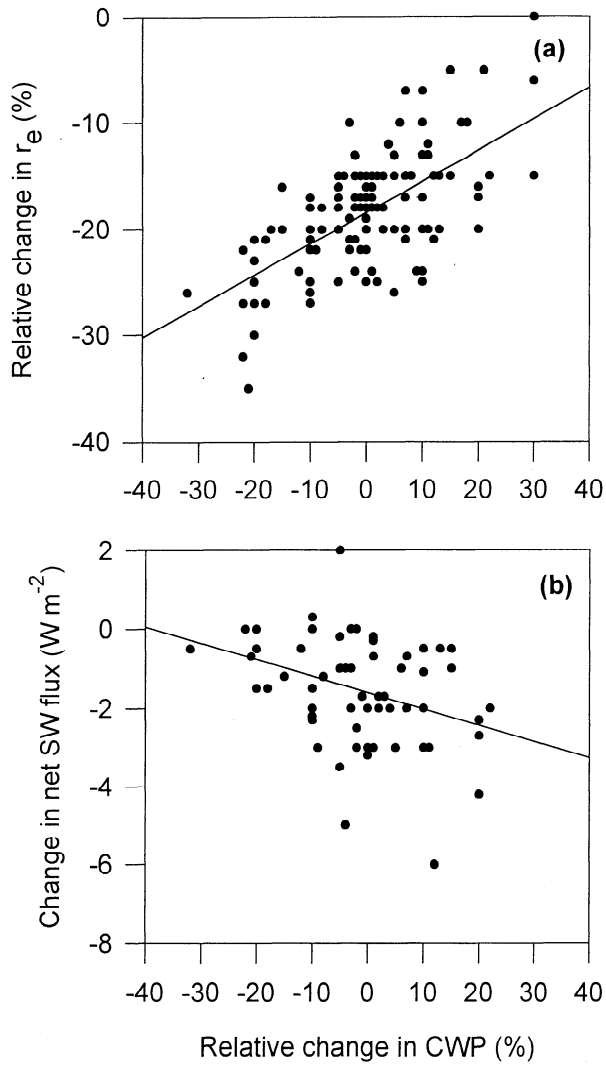

Figure 15. Scatterplot of (a) the relative change of the effective radius, $\delta r_e/r_e$, and the relative change of the CWP, and (b) the change of the net shortwave radiative flux, $\delta(\mathrm{SW_{net}})/\mathrm{SW_{net}}$ above clouds (z= 20 km) versus the relative change of the CWP for the time interval December 20-25, 1992. Values are horizontal averages.

ings during December 20-25, 1992, a 6-day case study. The predicted cloud variables and sulfate concentrations are used to estimate the impact of sulfate on radiative fluxes. The main findings are as follows.

1. The presence of convective clouds has a significant impact on the spatial and temporal distribution of sulfur species such as SO_2 and $SO_4^{(2-)}$. Thus SO_2 concentration tends to be significant in the upper troposphere due to convective pumping but with significant reduction in the free troposphere layer where the concentration of liquid water content in cloud droplets is maximum (between 2 and 6 km). SO_2 concentration in free troposphere can be ~10-20% of the average value at the surface. The $SO_4^{(2-)}$ particulate phase is depleted dramatically by nucleation scavenging, and the concentration above the BL can be as low as 10% of the value near the surface. The calculations indicate that $SO_4^{(2-)}$ in aqueous phase is the highest in convective towers in the layer 2-4 km.

2. When changing from a minimum to a maximum observed sulfate scenario in the tropical western Pacific area, the model indicates significant decrease of the effective radius of cloud droplet (up to ~2 μm), an increase in cloud droplet concentration (up to about 40 droplets per cm^3), and an increase of the sulfate in cloud water up to ~1 μg kg^{-1}. The sulfate distribution in the cloud field resembles the shapes of the cumulus clouds, with enhanced concentrations in updrafts and considerably decreased values in downdrafts.

3. The effect of sulfate increase between the two scenarios produces an average increase of the reflection of

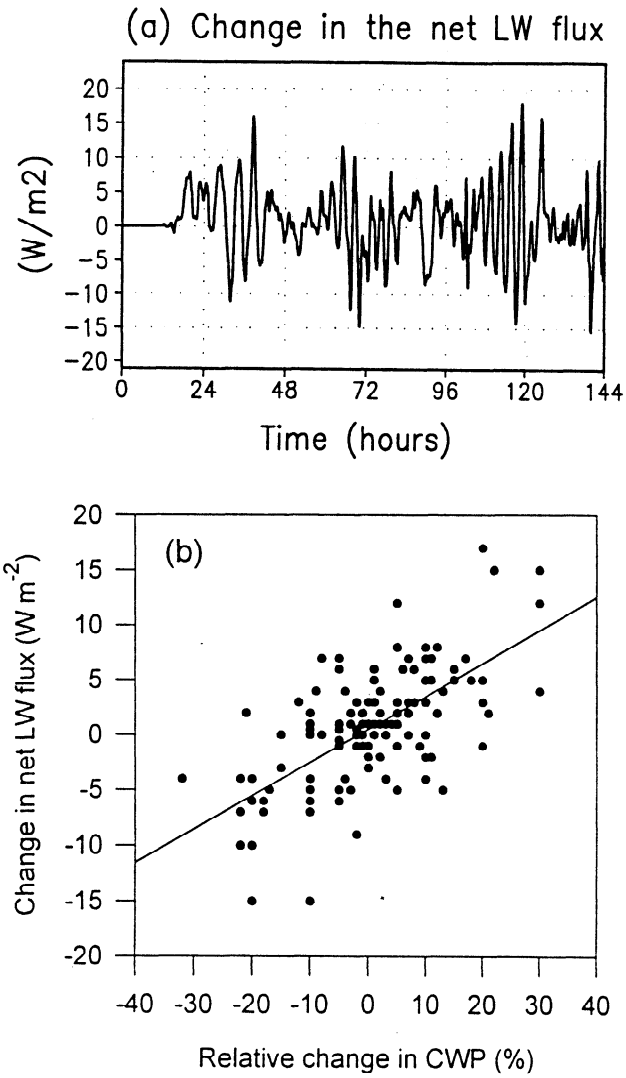

Figure 16. (a) Time evolution of the calculated horizontal average of the change in the net longwave radiative flux, $\delta(\mathrm{LW_{net}})$=$\mathrm{LW_{net}}$(run 2)-$\mathrm{LW_{net}}$(run 1), at the surface, for the time interval December 20-25, 1992. (b) Scatterplot of the $\delta(\mathrm{LW_{net}})$=$\mathrm{LW_{net}}$(run 2)-$\mathrm{LW_{net}}$(run 1) at the surface versus the relative change in CWP, for the time interval December 20-25, 1992. Values are horizontal averages.

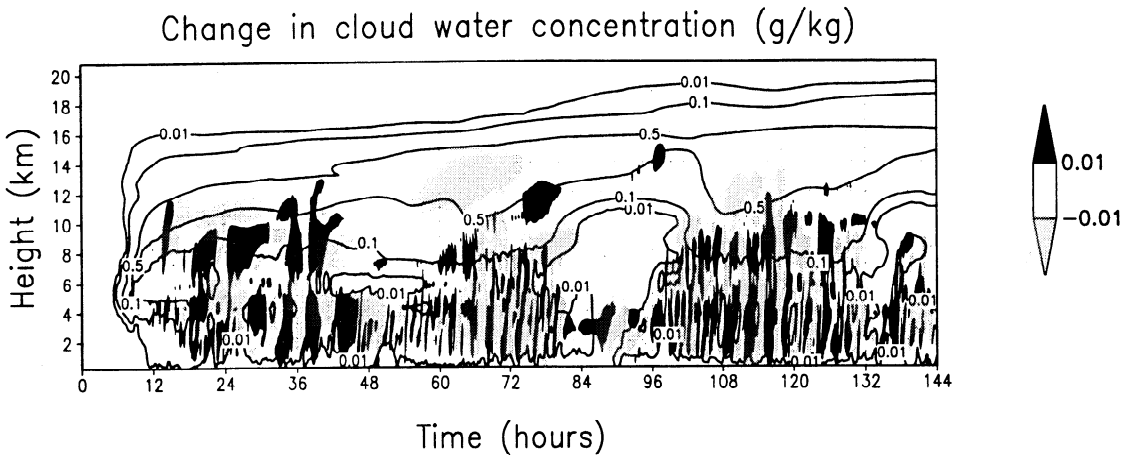

Figure 17. Time evolution of the calculated horizontal average of the changes in q_c, when the aerosol is changed from run 1 to run 2, for the time interval December 20-25, 1992. Only changes >0.01 g kg^{-1} in absolute value are shown. The solid lines indicate the absolute cloud water concentrations in the reference run.

SW radiation above the clouds. Time-horizontal averages of the differences between run 2 and run 1 of the net SW flux above clouds were estimated to be -1.5 W m^{-2} for daylight time intervals, with significant spatial and temporal variations. The horizontal average of the difference between run 2 and run 1 of the net SW flux above clouds reaches values typically about -3.0 W m^{-2} during the daylight. The difference between run 2 and run 1 of the net LW radiation flux near the Earth's surface has noticeable variations but the time-horizontal average is insignificant. The changes in the net LW flux between the two runs are accompanied by changes in air temperature (with magnitude of ~1°C) and by typical variations in the CWP of ~10-20%.

Our model enables us to explore the increase in variability of radiative fluxes at smaller scales and points out significant structure in the SW and LW flux changes in the cloudy domain induced by the aerosol increase. Such simulations are part of an effort to use high-resolution convective-cloud models with detailed cloud microphysics, aerosol, and chemistry to assess the role of convective clouds in the climate system. However, we must keep in mind that the results presented here are from a case study, and different scenarios, sensitivity studies, and validation with observations must be considered in order to assess the importance of convective clouds on the radiative changes caused by current or future aerosol increases and to incorporate these parameterizations in large-scale models.

Acknowledgments. The authors gratefully acknowledge Steve Krueger for providing the data from TOGA COARE used in this case study. The chemical data were obtained from the NASA Langley Research Center EOSDIS Distributed Active Archive Center (Doug Davis). We thank James Haywood, Stephen Klein, Brian Soden, Andrzej Klonecki, and two anonymous reviewers for their valuable comments and suggestions.

References

Ackerman, A. S., O. B. Toon, and P. V. Hobbs, Numerical modeling of ship tracks produced by injections of cloud condensation nuclei into marine stratiform clouds, *J. Geophys. Res., 100*, 7121-7133, 1995.

Andronache, C., L. J. Donner, V. Ramaswamy, C. J. Seman, and R. S. Hemler, The effects of atmospheric sulfur on the radiative properties of convective clouds: A limited area modeling study, *Geophys. Res. Lett., 25*, 1423-1426, 1998.

Blyth, A. M., and J. Latham, A climatological parameterization for cumulus clouds, *J. Atmos. Sci., 48*, 2367-2371, 1991.

Boucher, O., and U. Lohmann, The sulfate-CCN-cloud albedo effect: A sensitivity study with two general circulation models, *Tellus, Ser. B, 47B*, 281-300, 1995.

Boucher, O., and H. Rodhe, The sulfate-CCN-cloud albedo effect: A sensitivity study, *Rep. CM-83*, 20 pp., Dep. of Meteorol., Stockholm Univ., Stockholm, Sweden, 1994.

Chameides, W. L., and D. D. Davis, The free radical chemistry of cloud droplets and its impact upon the composition of rain, *J. Geophys. Res., 87*, 4863-4877, 1982.

Charlson, R. J., S. E. Schwartz, J. M. Hales, R. D. Cess, J. A. Coakley, J. E. Hansen, and D. J. Hofmann, Climate forcing by anthropogenic aerosols, *Science, 255*, 423-430, 1992.

Chatfield, R. B., and P. J. Crutzen, Sulfur dioxide in remote oceanic air: Cloud transport of reactive precursors, *J. Geophys. Res., 89*, 7111-7132, 1984.

Chin, M., and D. J. Jacob, Anthropogenic and natural contributions to atmospheric sulfate: A global analysis, *J. Geophys. Res., 101*, 18,691-18,699, 1996.

Chin, M., D. J. Jacob, G. M. Gardner, M. S. Foreman-Fowler, P. A. Spiro, and D. L. Savoie, A global three-dimensional model of tropospheric sulfate, *J. Geophys. Res., 101*, 18,667-18,690, 1996.

Chuang, C. C., and J. E. Penner, Effects of anthropogenic sulfate on cloud drop nucleation and optical properties, *Tellus, Ser. B, 47B*, 566-577, 1995.

Chuang, C. C., J. E. Penner, K. E. Taylor, A. S. Grosmann, and J. J. Walton, An assessment of the radiative effects of anthropogenic sulfate, *J. Geophys. Res., 102*, 3761-3778, 1997.

Dong, X., T. P. Ackerman, E. E. Clothiaux, P. Pilewskie,

and Y. Han, Microphysical and radiative properties of boundary layer stratiform clouds deduced from ground-based measurements, *J. Geophys. Res., 102*, 23,829-23,843, 1997.

Donner, L. J., C. J. Seman, and R. S. Hemler, Three-dimensional cloud-system modeling of GATE convection, *J. Atmos. Sci.*, in press, 1998.

Flossmann, A. I., The scavenging of two different types of marine aerosol particles calculated using a two-dimensional detailed cloud model, *Tellus, Ser. B, 43B*, 301-321, 1991.

Ghan, S. J., C. C. Chuang, and J. E. Penner, A parameterization of cloud droplet nucleation. I, Single aerosol type, *Atmos. Res., 30*, 197-221, 1993.

Giorgi, F., and W. L. Chameides, Rainout lifetimes of highly soluble aerosols and gases as inferred from simulations with a general circulation model, *J. Geophys. Res., 91*, 14,367-14,376, 1986.

Godfrey, J. S., R. A. Houze Jr., R. H. Johnson, R. Lukas, J.-L. Redelsperger, A. Sumi, and R. Weller, Coupled Ocean-Atmosphere Response Experiment (COARE): An interim report, *J. Geophys. Res., 103*, 14,395-14,450, 1998.

Han, Q., W. B. Rossow, and A. A. Lacis, Near-global survey of effective droplet radii in liquid water clouds using ISCCP data, *J. Clim., 7*, 465-497, 1994.

Haywood, J. M., and K. P. Shine, The effect of anthropogenic sulfate and soot on the clear sky planetary radiation budget, *Geophys. Res. Lett., 22*, 603-606, 1995.

Haywood, J. M., V. Ramaswamy and L. J. Donner, A limited-area-model case study of the effects of sub-grid scale variations in relative humidity and cloud upon the direct radiative forcing of sulfate aerosol, *Geophys. Res. Lett., 24*, 143-146, 1997.

Hegg, D. A., Cloud condensation nucleus-sulfate mass relationship and cloud albedo, *J. Geophys. Res., 99*, 25,903-25,907, 1994.

Hegg, D. A., and P. V. Hobbs, Measurements of sulfate production in natural clouds, *Atmos. Environ., 16*, 2663-2668, 1982.

Hegg, D. A., S. Rutledge, and P. V. Hobbs, A numerical model for sulfur chemistry in warm-frontal rainbands, *J. Geophys. Res., 89*, 7133-7147, 1984.

Hegg, D. A., R. J. Ferek, and P. V. Hobbs, Light scattering and cloud condensation nucleus activity of sulfate aerosol measured over the northeast Atlantic Ocean, *J. Geophys. Res., 98*, 14,887-14,894, 1993.

Hegg, D. A., R. Majeed, P. F. Yuen, M. B. Baker, and T. V. Larson, The impacts of SO_2 oxidation in cloud drops and in haze particles on aerosol light scattering and CCN activity, *Geophys. Res. Lett., 23*, 2613-2616, 1996.

Held, I. M., R. S. Hemler, and V. Ramaswamy, Radiative-convective equilibrium with explicit two-dimensional moist convection, *J. Atmos. Sci., 50*, 3909-3927, 1993.

Hobbs, P. V., *Aerosol-Cloud-Climate Interactions, Int. Geophys. Ser., vol. 54*, 223 pp., Academic, San Diego, Calif., 1993.

Hoell, J. M., D. D. Davis, S. C. Liu, R. Newell, H. Akimoto, R. J. McNeal, and R. J. Bendura, The Pacific Exploratory Mission-West, Phase B: February-March, 1994, *J. Geophys. Res., 102*, 28,223-28,239, 1997.

Holton, J., *An Introduction to Dynamic Meteorology*, 391 pp., Academic, San Diego, Calif., 1979.

Intergovernmental Panel on Climate Change (IPCC), *Climate Change 1994*, edited by J. T. Houghton et al., 339 pp., Cambridge Univ. Press, New York, 1995.

Jones, A., and A. Slingo, Predicting cloud droplet effective radius and indirect sulfate aerosol forcing using a general circulation model, *Q. J. R. Meteorol. Soc., 122*, 1573-1595, 1996.

Kiehl, J. T. and B. P. Briegleb, The relative roles of sulfate aerosols and greenhouse gases in climate forcing, *Science 260*, 311-314, 1993.

King, M. D., F. F. Radke, and P. V. Hobbs, Optical properties of marine stratocumulus clouds modified by ships, *J. Geophys. Res., 98*, 2729-2739, 1993.

Kreidenweis, S. M., Y. Zhang, and G. R. Taylor, The effects of clouds on aerosol and chemical species production and distribution, 2, Chemistry model description and sensitivity analysis, *J. Geophys. Res., 102*, 23,867-23,882, 1997.

Langner, J., and H. Rodhe, A global three-dimensional model of the tropospheric sulphur cycle, *J. Atmos. Chem., 13*, 255-263, 1991.

Leaitch, W. R., and G. A. Isaac, On the relationship between sulfate and cloud droplet number concentration, *J. Clim., 7*, 206-212, 1994.

Leaitch, W. R., G. A. Isaac, J. W. Strapp, C. M. Banic, and H. A. Wiebe, The relationship between cloud droplet number concentrations and anthropogenic pollution: observations and climatic implications, *J. Geophys. Res., 97*, 2463-2474, 1992.

Lin, X., and R. H. Johnson, Kinematic and thermodynamic characteristics of the flow over the Western Pacific warm pool during TOGA COARE, *J. Atmos. Sci., 53*, 695-715, 1996.

Lin, X., W. L. Chameides, C. S. Kiang, A. W. Stelson, and H. Berresheim, A model study of the formation of cloud condensation nuclei in remote marine areas, *J. Geophys. Res., 97*, 18,161-18,171, 1992.

Lipps, F. B., and R. S. Hemler, Numerical simulation of deep tropical convection associated with large-scale convergence, *J. Atmos. Sci., 43*, 1796-1816, 1986.

Lohmann, U., and J. Feichter, Impact of sulfate aerosols on albedo and lifetime of clouds: A sensitivity study with the ECHAM4 GCM, *J. Geophys. Res., 102*, 13,685-13,700, 1997.

Lord, S. J., H. E. Willoughby, and J. M. Pietrowicz, Role of parameterized ice-phase microphysics in axisymmetric, non-hydrostatic tropical cyclone model, *J. Atmos. Sci., 41*, 2836-2848, 1984.

Marshall, J. S., and W. M. Palmer, The distribution of raindrops with size, *J. Meteorol., 5*, 165-166, 1948.

Martin, L. R., and D. E. Damschen, Aqueous oxidation of sulfur dioxide by hydrogen peroxide at low pH, *Atmos. Environ., 15*, 1615-1621, 1981.

Martin, G. M., D. W. Johnson, and A. Spice, The measurements and parameterizations of effective radius of droplets in warm stratocumulus clouds, *J. Atmos. Sci., 51*, 1823-1842, 1994.

McFarquhar, G. M., and A. J. Heymsfield, The definition and significance of an effective radius for ice clouds, *J. Atmos. Sci., 55*, 2039-2052, 1997.

Moncrieff, M. W., S. K. Krueger, D. Gregory, J. Redelsperger, and W. Tao, GEWEX Cloud System Study (GCSS) working group 4: Precipitating convective cloud systems, *Bull. Am. Meteorol. Soc., 78*, 831-845, 1997.

Pandis, S. N., L. M. Russell, and J. H. Seinfeld, The relationship between DMS flux and CCN concentration in remote marine regions, *J. Geophys. Res., 99*, 16,945-16,957, 1994.

Penkett, S. A., and J. A. Garland, Oxidation of sulphur dioxide in artificial fogs by ozone, *Tellus, 26*, 284-290, 1974.

Penner, J. E., R. J. Charlson, J. M. Hales, N. S. Laulainen, R. Leifer, T. Novakov, J. Ogren, L. F. Radke, S. E. Schwartz, and L. Travis, Quantifying and minimizing uncertainties of climate forcing by anthropogenic aerosols, *Bull. Am. Meteorol. Soc., 75*, 375-399, 1994.

Pontikis, C., and E. Hicks, Contribution to the cloud droplet effective radius parameterization, *Geophys. Res. Lett. 19*, 2227-2230, 1992.

Pruppacher, H. R., The microstructure of atmospheric clouds and precipitation, in *Clouds, Their Formation, Optical Properties, and Effects*, edited by P. V. Hobbs and A. Deepak, 497 pp., Academic, San Diego, Calif., 1981.

Pruppacher, H. R., and J. D. Klett, *Microphysics of Clouds and Precipitation*, pp. 714, Norwell, Mass., 1978.

Quinn, P. K., D. S. Covert, T. S. Bates, V. N. Kapustin, D. C. Ramsey-Bell, and L. M. McInnes, Dimethylsulfide/cloud condensation nuclei/climate system: Relevant size-resolved measurements of the chemical and physical properties of the atmospheric aerosol particles, *J. Geophys. Res., 98*, 10,411-10,427, 1993.

Ramaswamy, V., and J. T. Kiehl, Sensitivities of the radiative forcing due to large loadings of smoke and dust aerosols, *J. Geophys. Res., 90*, 5597-5613, 1985.

Russell, L. M., S. N. Pandis, and J. H. Seinfeld, Aerosol production and growth in the marine boundary layer, *J. Geophys. Res., 99*, 20,989-21,003, 1994.

Seigneur, C., and P. Saxena, A theoretical investigation of sulfate formation in clouds, *Atmos. Environ., 22*, 101-115, 1988.

Short, D. A., P. A. Kucera, B. S. Ferrier, J. C. Gerlach, S. A. Rutledge, and O. W. Thiele, Shipboard radar rainfall patterns within TOGA/COARE IFA, *Bull. Am. Meteorol. Soc., 78*, 2817-2836, 1997.

Slingo, A., A GCM parameterization for shortwave radiative properties of water clouds, *J. Atmos. Sci., 46*, 1419-1427, 1989.

Talbot, R. W., et al., Chemical characteristics of continental outflow from Asia to the troposphere over the western Pacific Ocean during February-March 1994: Results from PEM-West B, *J. Geophys. Res., 102*, 28,255-28,274, 1997.

Taylor, G. R., S. Kreidenweis, and Y. Zhang, The effects of clouds on aerosol and chemical species production and distribution, 1 Cloud model formulation, mixing, and detrainment, *J. Geophys. Res., 102*, 23,851-23,865, 1997.

Thornton, D. C., A. R. Bandy, B. W. Blomquist, J. D. Bradshaw, and D. R. Blake, Vertical transport of sulfur dioxide and dimethyl sulfide in deep convection and its role in new particle formation, *J. Geophys. Res., 102*, 28,501-28,509, 1997a.

Thornton, D. C., A. R. Bandy, B. W. Blomquist, R. W. Talbot, and J. E. Dibb, Transport of sulfur dioxide from the Asian Pacific Rim to the North Pacific troposphere, *J. Geophys. Res., 102*, 28,489-28,499, 1997b.

Twomey, S. A., Pollution and the planetary albedo, *Atmos. Environ., 8*, 1251-1256, 1974.

Twomey, S. A., The influence of pollution on the shortwave albedo and clouds, *J. Atmos. Sci., 34*, 1149-1152, 1977.

Twomey, S. A., Aerosols, clouds and radiation, *Atmos. Environ., Part A, 25*, 2435-2442, 1990.

Van Dingenen, R., F. Raes, and N. J. Jensen, Evidence for anthropogenic impact on number concentration and sulfate content of cloud-processed aerosol particles over the North Atlantic, *J. Geophys. Res., 100*, 21,057-21,067, 1995.

Wang, C., and J. S. Chang, A three-dimensional numerical model of cloud dynamics, microphysics, and chemistry, 1, Concepts and formulation, *J. Geophys. Res., 98*, 14,827-14,844, 1993.

Wang, C., and P. J. Crutzen, Impact of a simulated severe local storm on the redistribution of sulfur dioxide, *J. Geophys. Res., 100*, 11,357-11,367, 1995.

Wang, C., P. J. Crutzen, V. Ramanathan, and S. F. Williams, The role of deep convective storm over the tropical Pacific Ocean in the redistribution of atmospheric chemical species, *J. Geophys. Res., 100*, 11,509-11,516, 1995.

Warren, S. G., C. J. Hahn, J. London, R. M. Chervin, and R. L. Jenne, Global distribution of total cloud cover and cloud type amounts over land, *NCAR Tech. Note, DOE/ER/60085-H1, NCAR/TN-273+STR*, Natl. Cent. for Atmos. Res., Boulder, Colo., 1986.

Warren, S. G., C. J. Hahn, J. London, R. M. Chervin, and R. L. Jenne, Global distribution of total cloud cover and cloud type amounts over ocean, *NCAR Tech. Note, DOE/ER-0406, NCAR/TN-317+STR*, Natl. Cent. for Atmos. Res., Boulder, Colo., 1988.

Webster, J. P., and R. Lukas, TOGA COARE: The coupled ocean-atmosphere response experiment, *Bull. Am. Meteorol. Soc., 73*, 1377-1416, 1992.

Wu, X., W. W. Grabowski, and M. W. Moncrieff, Long-term behavior of cloud systems in TOGA COARE and their interaction with radiative and surface processes, I, Two-dimensional modeling study, *J. Atmos. Sci., 55*, 2693-2714, 1998.

Xiao, H., G. R. Carmichael, J. Durchenwald, D. Thornton, and A. Bandy, Long-range transport of SOx and dust in East Asia during the PEM B experiment, *J. Geophys. Res., 102*, 28,589-28,612, 1997.

C. Andronache, L. J. Donner, C. J. Seman, V. Ramaswamy, and R. S. Hemler, GFDL/NOAA, Princeton University, Forrestal Campus, U.S. Route 1, P.O. Box 308, Princeton, NJ 08542. (e-mail: cna@gfdl.gov)

(Received June 13, 1998; revised October 28, 1998; accepted November 5, 1998.)